Photovoltaic Performance of P3HT:SWCNT:PCBM based Bulk Heterojunction Solar Cell

Submitted by

Saad Mohammed Khan (11221024)

Ajnan Aron Hasan (11221058)

Avizet Saha (11221042)

A Thesis

Submitted as the Partial Fulfilment for the Degree of

Bachelor of Science in Electrical and Electronic Engineering

Department of Electrical and Electronic Engineering

BRAC University

Dhaka-1212, Bangladesh

CERTIFICATE OF APPROVAL

The thesis entitled **"Photovoltaic Performance of P3HT:SWNT:PCBM based Bulk Heterojunction Solar Cell"** submitted by **Saad Mohammed Khan**, **Ajnan Aron Hasan**, **Avizet Saha** has been accepted satisfactory in partial fulfilment of the requirement for the degree of Bachelor of Science in Electrical and Electronics Engineers on December , 2015

Supervisor

_____

(Dr. Sharif Mohammad Mominuzzaman)
Professor

Department of Electrical and Electronic Engineering

Bangladesh University of Engineering and Technology (BUET)

CANDIDATE DECLARATION

It is hereby declared that this thesis or any part of it has not been submitted elsewhere for the award of any degree or diploma.

Author

_____

Saad Mohammed Khan

Author

_____

Ajnan Aron Hasan

Author

_____

Avizet Saha

ACKNOWLEDGEMENT

We are grateful to the Almighty for directing us toward the right path in order to pursue the requirement of the full thesis work.

There are some people we would like to thank who have helped us in our research. First and foremost we would like to express our gratitude towards our respected thesis supervisor, **Dr. Sharif Mohammad Mominuzzaman,** Professor of EEE department BUET, for his insight and direction. His faith in us and motivation has provided us with the confidence to achieve our goals.

We would also like to thank **Sabbir Ahmed Khan** who referred our group to Professor Mominuzzaman and always believed in our abilities.

Lastly, we are ever grateful to our Parents and well-wishers for supporting and encouraging us throughout the work.

TABLE CONTENTS

LIST OF FIGURES

LIST OF TABLE

Abbreviations

OSC	**Organic Solar Cells**
OPV	**Organic Photovoltaic**
BHJ	**Bulk Hetero Junction**
Jsc	**Short Current Density**
Voc	**Open circuit Voltage**
FF	**Fill Factor**
PCE	**Power Conversion Efficiency**
SWCNT	**Single Wall Carbon Nanotube**
P3HT	**Poly (3-hexylthiophene)**
PCBM	**(6,6)-Phenyl C61 Butyric acid Methyl ester**
PEDOT:PSS	**Poly(3,4-ethylenedioxythiophene) Polystyrene Sulfonate**
ITO	**Indium Tin Oxide**
HOMO	**Highest Occupied Molecular Orbital**
LUMO	**Lowest Unoccupied Molecular Orbital**
Am1.5	**Air Mass**

ABSTRACT

Organic photovoltaic cells are believed to be the ideal alternative to silicon based solar cell devices due to its low cost, ease of fabrication and high mechanical flexibility. However, despite possessing such astounding properties their application in the main stream market has been limited due to its low PCE. The efficiency of bulk heterojunction solar cell is limited primarily due to the low carrier mobility of the polymer and the active layer's incapability to absorb photon wavelengths in the NIR region. SWCNTs are known to have high carrier mobility due its ballistic property and can also absorb photon wavelengths in the NIR region. This fascinating optical and electrical property of SWCNT makes them a promising material as an additive to a Polymer: Fullerene based active layer composite. In this work we examine the influence of SWCNT on the absorption spectra and the J-V characteristics of P3HT: PCBM based bulk heterojunction solar cell. The optical simulation of the bulk heterojunction solar cell was carried out using the optical transfer matrix methodology while analytical solutions of 1D drift-diffusion equation were used to predict the J-V characteristics of the organic photovoltaic device. The optical simulation result show that the incorporation of SWCNT to the P3HT: PCBM active layer composite widens the absorbance spectrum by increasing the absorption coefficient in the UV and as well as infra-red region. The result obtained from the J-V curve show that the photovoltaic performance of the P3HT: PCBM solar cell devices depend on the concentration of SWCNT. The incorporation of the 1% SWCNT improved the Jsc by 10%. The Voc at 1wt% SWCNT remained relatively the same while the power conversion efficiency enhanced by 34%.

Chapter 1

Introduction

1.1 Solar Energy

The need to produce electrical energy from renewable sources has become more intense in the last few years primarily due to the exhaustive and harmful nature of fossil fuels and other non-renewable sources. The use of renewable energy as the most prominent source of energy still remains a challenge. Most of the renewable sources of energy are sporadic in nature and are also situated in geographically constricted locations. The presence of such drawbacks have made renewable energy sources financially less feasible to their non-renewable counterparts notably fossil fuels. One of the most studied from of renewable energy is the solar energy. Solar energy is free in nature. It does not produce any form of harmful waste.it can be easily converted to any form of energy and is ecologically acceptable. The energy produced by sun in one hour is more than enough to meet the per annum demand of world energy [32]. Such compelling features of solar energy has led to the use of photovoltaic systems. Initially high costs and low conversion efficiency have been the major obstruction in making photovoltaic systems the primary energy producing technology but the PCE has improved drastically in the last few years thanks advance research methodologies and modern technologies leading to a greater interest in the study of photovoltaic systems.

1.2Background and Present State of The Problem

Organic solar cells are a fascinating alternative of conventional solar cells, due its low fabrication cost, high mechanical flexibility [31]. Despite possessing such promising features, OSC's still display low PCE primarily due to low carrier mobility, short exciton diffusion length and limited absorbance spectrum [13]. One way to improve the PCE is to use an active layer based on bulk heterojunction. The introduction of bulk-heterojunction solar cell has resulted in improved PCE [10]. For OPV's to rival its inorganic counter parts further improvement in PCE required. SWCNTs possess high carrier mobility with addition to the capability to absorb photons in the NIR region [5]. The effective hole mobility of P3HT: SWCNT increase up to certain ratio (usually <1wt% SWCNT) due the presence of defects and impurities and hence the full potential of SWCNTS as active composite has never been fully understood [26, 27].

To understand the full potential SWCNT as an active layer additive requires thorough simulation based study, various analytical modelling techniques based on Poisson-continuity equations considering Generation rates and mobility effects are proposed by researchers[7,8,5]. Such models can be modified to fully realize the potential of SWCNT in the field of organic photovoltaics.

1.3 Objectives

The objectives of this thesis are to:

- Simulate the performance of P3HT:PCBM based BHJ solar cells
- Simulate the effect of SWCNT on the Optical profile of P3HT:PCBM based BHJ solar cell
- Simulate the effect of SWCNT on the J-V characteristics of P3HT:PCBM based BHJ solar cell
- Simulate the effect of pure s-SWCNT on the J-V characteristics of P3HT:PCBM based BHJ solar cell

1.4 Thesis Layout

The thesis has been divided into four chapters. Chapter 1 provides general in-formation followed by background, present state of the problem and objectives of the thesis work.

Chapter two covers about organic solar cells, the types of organic solar cells, working principle of organic solar cells, materials used in the active layer of an Organic solar cell and also provides a detailed literature study of the impact SWCNT has had on the performance of Organic solar cell over the years.

Chapter three explains the model's used to simulate the characteristics of an Organic solar cell. In the optical model section, transfer matric theory is used for the calculation of photon absorption. After that an analytical model which couples Poisson and continuity equation considering the charge carrier generation, exciton dissociation and charge carrier recombination is explained in detail.

Chapter four provides the results attained from the simulation and analyses the results obtained.

Chapter five provides conclusive discussions for this work. Some scope for the future work in relation with the present work is also presented.

Chapter 2

Review of Organic Solar Cells

2.1 Why Organic Solar Cells?

The material cost of OSC's active layers is relatively very cheap when compared to its inorganic materials. Moreover, OSC's have higher absorption coefficient and thus can have a thinner active layer than its inorganic counter parts. Unlike crystalline solar cells which needs to have a very vigorous and costly fabrication process to attain high purity, organic solar cells undergo a relatively less complicated and cost effective process.[31]

2.2 Types of Organic Solar Cells

2.2.1 Bilayer Organic Solar Cells

Exciton gets created within the active layer upon the absorption of light. The exciton generated then diffuses to the donor acceptor interface where it gets dissociated owing to the junction energy leading to the formation of an EHP. The generated carrier now drifts towards their respective electrodes resulting in electrical current. Since exciton diffusion length is very small in comparison to the layer thickness most of the generated carriers end up recombining leading to a very low PCE [21].

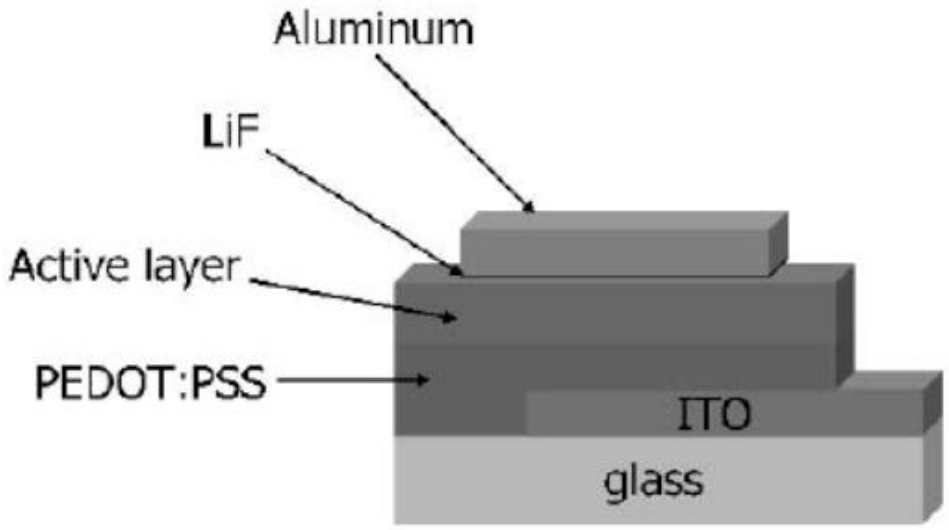

Fig 2.1: Common Device Structure for an Organic Solar Cell [21]

2.2.2 Bulk Heterojunction Organic Solar Cells

One way to improve the PCE of an OSC is to increase the number of DA interfaces available for the dissociation of excitons by mixing the donor and acceptor molecules of the active layers in a random fashion. This type of OSC's are called bulk heterojunction solar cell. The obtained PCE of a BHJ is usually much larger than bi-layer devices. The larger PCE is due to the increase in exciton dissociation probability which gets enhanced due to increase in the number of interface available for the dissociation of exciton [21].

2.3Organic Solar Cell Working Principle

The four principle steps involved in the generation of photocurrents are:

1) **Photon Absorption:** For a BHJ solar cell both the donor and acceptor are involved in the absorption of light. The absorption of photon by the active layer results in the formation of an exciton which does not get directly dissociated into an EHP due to the low dielectric permittivity of the active layer composite.

2) **Exciton Diffusion to junction:** The generated exciton now diffuses towards the junction to get successfully dissociated into free charge carriers.

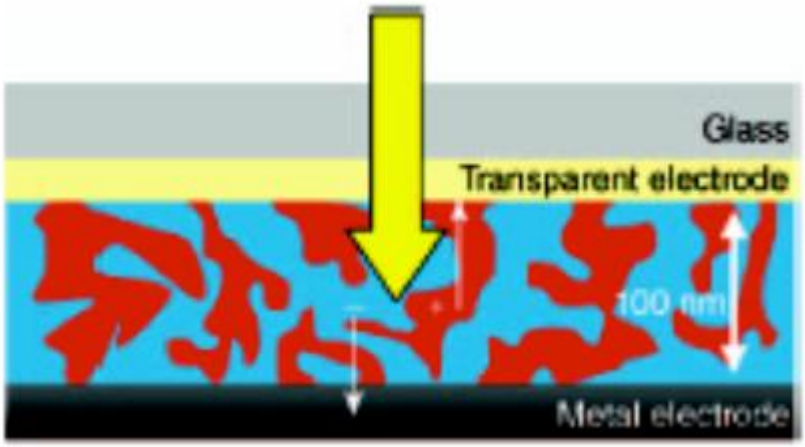

Fig 2.2Schematic Diagram of Bulk Heterojunction.[22]

3) Charge Separation: Once the exciton gets generated, it needs to get dissociated into a free charge carrier. The multiple DA interfaces available due to the random mixture of donor and acceptor helps to dissociate the exciton into free EHP.

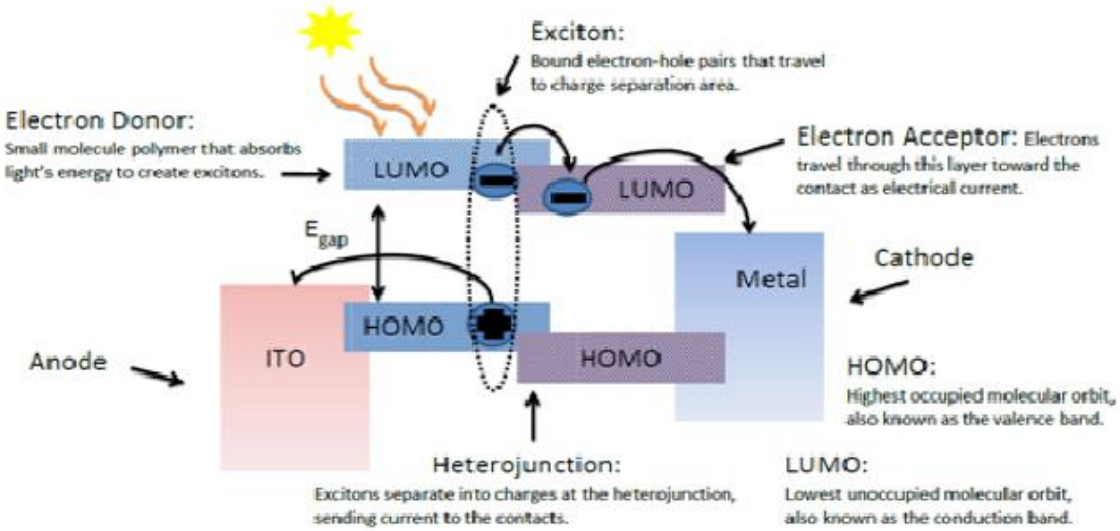

Fig 2.3: Operation of Organic Solar Cell. (www.marblar.com)

4) Charge Transport: Charge transport is the last step in the photo current generation process where the separated charges drift to their respective electrodes through the applied electric field which is generated in the active layer as a result of the difference between the electrode work function. [20][21][22]

2.4Optical and Electrical Properties of Active Layer Components

2.4.1 PCBM and its Properties:

Fullerene C60 exhibits good electron mobility and has well-symmetric structure. One molecule of C60 has the ability to attract four electrons making them a popular choice as acceptor materials in Organic solar cells. C60's limited solubility in organic solvents and its tendency to form severe phase segregation in the D/A interface lead to the use of [6, 6]-phenyl-C61-butyric acid methyl ester ($PC_{60}Bm$) as acceptor in OPVs [19]. $PC_{60}BM$ and its corresponding C70 derivative ($PC_{70}BM$) have been prevailingly used as acceptor in OPVs.Compared to $PC_{60}BM$, $PC_{70}BM$ possesses a stronger absorption in visible range [32]. However, C70 is much more expensive than that of C60 because of its tedious purification process [32]. The molecular structures and the synthetic route of $PC_{60}BM$ and $PC_{70}BM$ are shown in fig 2.13. $PC_{60}BM$ and $PC_{70}BM$ absorption spectra are shown in Fig 2.3. It can be observed that both materials display strong absorption at ultraviolet region, from 200 to 400 nm with $PC_{70}BM$ possessing a stronger absorption in visible region than $PC_{60}BM$ which results in greater Jsc and PCE.

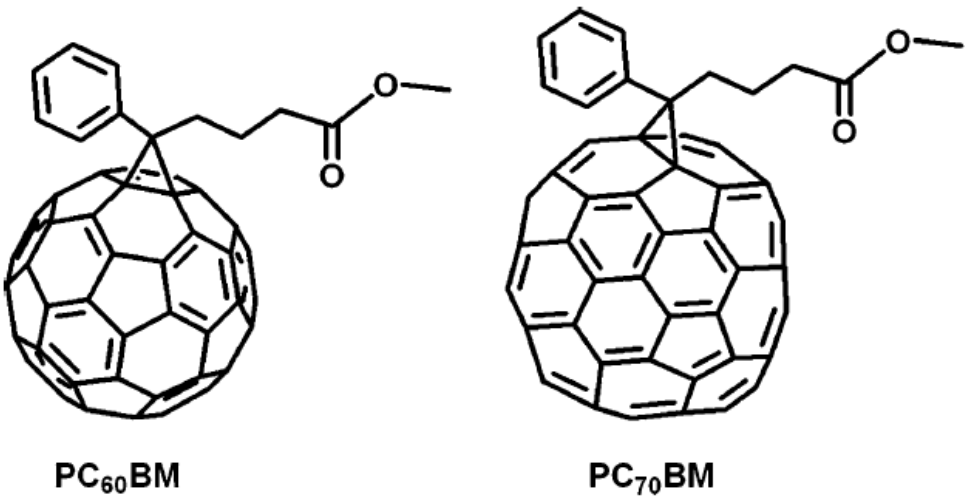

Fig 2.4: Molecular Structures of PC_{60}BM and P$C_{70}BM$.[15]

The electrochemical properties and energy level of the fullerene derivatives are very important for PSCs. The difference between the LUMO energy level of the fullerene acceptors and HOMO energy level of the polymer donor [15, 16] determines the open circuit voltage (Voc). Hence in order to match with a polymer HOMO, the LUMO energy level of fullerene derivatives is very influential factor for the application of an acceptor in OPV's. LUMO level of unsubstituted C_{60} and PCBM are known to be around -4.2and -4.0ev respectively [17, 18]. Addition of substituent has the ability to elevate the LUMO level of unsubstituted C_{60}. The LUMO level of bis-PCBM is known to be about 0.1-0.15eV higher than that of P3HT:PCBM based devices [23]. Higher Voc can also be realized with the use of multi-adducts in OPVs. Despite elevating the LUMO level, substituents of PCBM are inert for electron transport. The presence of bi and multi-adducts also causes the weakening of symmetric properties of fullerene making them an unfavourable choice for the purpose of acceptors [19]. PCBM PC_{60}BM and PC_{70}BM are hence still the best electron acceptors in the OPV.

2.4.2 SWCNT and its Properties:

Generally, the properties of a carbon nanotube are dependent on its structure. Their optical and electrical properties can be tuned by varying the range of band gap from semiconducting to metallic. This particular ability of CNT is not possessed by any other nanoscopic form of carbon such as fullerenes. The electronic property of SWNT highly depends on its chirality, chiral indices (n, m) determine whether particular CNT is metallic or semiconducting in nature. If the relation between the chiral indices are n-m=3j where j=0 then the CNT can be considered as metallic; if j≠0 then it will be considered as semi-metallic. CNTs will be considered semiconducting if the relation between chiral indices are n-m=3j±1. If CNTs chiral indices are equal (n=m), it denoted as "armchair". CNTs with chiral indices (n,0) are called "zig-zag". The 1D structure of SWCNTs give rise to a characteristic called the van Hove singularities in the DOS diagram. The absorption spectra of SWCNTs are dictated by the van Hove singularities, showing peaks or spikes during the electronic transition. In spite of its spare structure, the thickness between 10-100nm is showing high transmittance within the visible spectrum. The thermal excitation promotes its carries to the conduction band which shows a highly temperature dependency of SWNT. SWCNTs show ballistic transport properties leading to high carrier motilities (100000 cm^2 Vs^{-1}) and astounding transport properties such as high electrical conductivity along their primary axial co-ordinate (1000÷200000 Scm^{-1}). The high aspect ratio (up to 10^6) further enhances the electrical conductivity.SWCNTs are generally p type materials but their electronic property might change with the introduction of defects into its electronic structure. The introduction of defects to manage electronic properties can be used to develop powerful organic electronics based devices The work function of m-SWCNTs is independent of its chirality and increases marginally with diameter. Contrariwise for s-SWCNTs, the work function decreases with

increasing tube diameter. Annealing or chemical doping tunes the work function and contact resistance of SWCNT [33, 34,5].

2.4.3 P3HT and its Properties:

In the world of Organic photovoltaics, the most vigorously studied polymer for the application in the field of BHJ solar cell is P3HT. P3HT is well known for its high regioregularity (> 95%), a requirement for high efficient performance of photovoltaic process. P3HT dominantly absorbs photons of wavelength in the region of 400-600 nm, and thus needs additional incorporation of layers with broader absorbance spectrum [32].

2.5Literature Review:

The pace at which OSC's has evolved in the last few years is fascinating. For a topic which had its first general device model published in the year 2005, OSC's have made huge progress in increasing its efficiency from a mere 0.04% in 1999 to 10.7% in 2010 [27]. Further improvement in the PCE was brought through the introduction of nano materials such as CNT and graphene as active layer materials. The introduction of CNT to the active layer materials in right proportions improved the morphology by increasing the crystallinity and ordering of the polymer and fullerene composites [29]. It also improved the carrier mobility and absorptivity of the active layer materials with limited absorbance spectrum [5]. CNT based bulk heterojunction solar cell devices have shown efficiencies up to 9.98% [9] and further research is taking place to improve the efficiency to a higher degree by chemically treating the CNTs with surfactants. N-doped and B-Doped CNTs have shown great capabilities in improving the PCE to the standard 10% limit. Doping MWCNT with nitrogen and boron improved the PCE to a highest 8.6% by introducing exciton dissociation centres and charge transfer channels [10]. N-doped and B-Doped SWCNTS are known to selectively

enhance the electron and hole transport carrying capability of the active layer involved in the photo generation process. The enhancement in hole mobility and electron mobility have enhanced the efficiency by 37% [11]. Quantum dot/N-doped CNTs have also been used in literature to improve the efficiency of a polymer: fullerene composite by 31%. which is a result of the enhancing of exciton dissociation and charge transport [13]. SWCNT hybrid's such as plasmonic metal-CNT hybrids have improved the PCE of OSC's to 9.98% by synergistic concurrent enhancement of charge generation, dissociation and transport in organic solar cells [9]. SWCNTS have also shown great performance as HTL. Hybrid P3HT-SWCNT based HTL's have improved the FF of P3HT: PCBM and PTB7: PCBM solar cells by 12 %and 32|% respectively resulting in 19.57%and 35.52% enhancement in PCE [12].

2.6 Solar cell Parameters

For solar cell characteristics, current- voltage curve is obtained first. From that curve different parameters are obtained. Each of this parameter will be described below:

2.6.1 Short Circuit Current Density (Jsc)

The short circuit density is the current density when the applied voltage is zero, the same condition as two electrodes of the cell being short circuited together. No power is induced at this point, but the Jsc will mark the onset power generation. In ideal devices, the Jsc will be same as the photo current density. However, it will be seen later that several effects can lower the Jsc from ideal values.

2.6.2Open Circuit Voltage (Voc)

The open circuit voltage is the voltage across the solar cell when the current density is equal to zero, which is the same as device being open circuited. Because J=0, and power is the

product of current and voltage no power is actually produced at this voltage. However the Voc marks the boundary for voltages at which power cab be produced, the open circuit voltage can also be thought of as the point at which the photocurrent generation and dark current processes compensated one another.

2.6.3Fill Factor (FF)

While Voc and Jsc mark the boundaries of power production in a solar cell, the maximum power density produced Pmax occurs at the voltage Vmax and the current density Jmax where the product of J and V is at a minimum. Because of the diode behaviour the additional resistance and recombination losses, Jmax and Vmax are always less than Jsc and Voc respectively. FF is an indication of how close Jmax and Vmax come to the boundaries of power production of jsc and Voc and also indicates the sharpness of bend in the exponential-V curve. Since higher FF means higher maximum power, High FF is desired. Now it is evident from the fact that Jmax and Vmax is always less than Jsc and Voc, FF is always less than one

2.6.4Power Conversion Efficiency (PCE)

The most discussed performance parameter of a solar cell is the power conversion efficiency (PCE) and is defined as the percentage of incident irradiation Pin that is converted into output power.

Chapter 3

Model Physics and Process of Calculation

3.1Optical Modelling:

The optical transfer matric methodology was used to simulate the performance of a BHJ solar cell [7].The model considers that in a thin film device, light is at normal incidence to the substrate. As shown in fig.1, a plane wave was incident from left at an m layer structure (layer 1 to layer m) between a semi-infinite transparent ambient and semi-infinite substrate. The resultant optical electric field due to the interference effect in the thin film device at any point x in layer j is a complex quantity and consists of a positive component $E_j^+(x)$ and a negative component $E_j^-(x)$, the optical properties of each layer (j) can be described by the complex index of refractions $\tilde{n_j} = n_j + ik_j$ and thickness d_j.

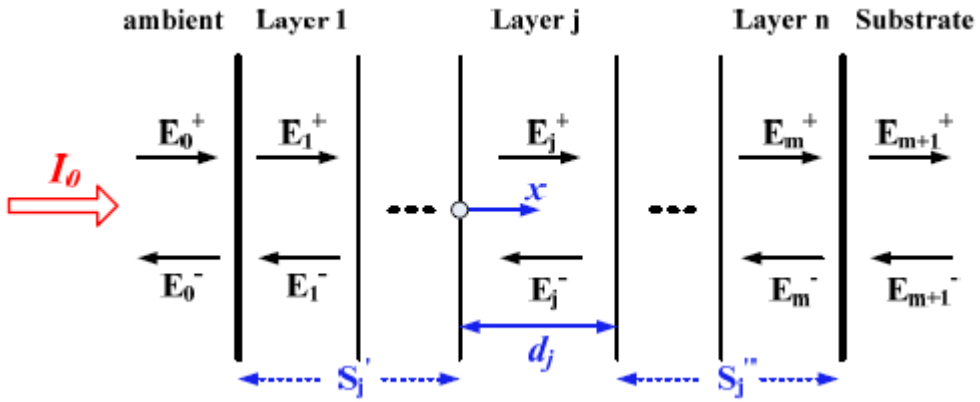

Fig 3.1: Schematic of m-layer Structure Between Ambient and Substrate. [7]

The two matrix that defines optical transfer matrices are 1) an interface matrix which describes each interfaceI_{jk}; 2) the layer matrix describing the propagation through layer j.

The behavior of light at the interface between j and k=j+1 layers can then be described by a 2×2 matrix containing the complex Fresnel coefficients. The interface matrix I_{jk} can be expressed as:

$$I_{jk} = \begin{bmatrix} (\widetilde{n_j} + \widetilde{n_k})/2\widetilde{n_j} & (\widetilde{n_j} - \widetilde{n_k})/2\widetilde{n_j} \\ (\widetilde{n_j} - \widetilde{n_k})/2\widetilde{n_j} & (\widetilde{n_j} + \widetilde{n_k})/2\widetilde{n_j} \end{bmatrix} \quad \text{.....(3.1.1)}$$

The layer matrix L_j is expressed as:

$$L_j = \begin{bmatrix} \exp(-i\frac{2\pi\widetilde{n_j}}{\lambda} . d_j) & 0 \\ 0 & \exp(-i\frac{2\pi\widetilde{n_j}}{\lambda} . d_j) \end{bmatrix} = \begin{bmatrix} \exp(-ik_{j\,.\,d_j}) & 0 \\ 0 & \exp(-ik_{j\,.\,d_j}) \end{bmatrix} \text{...(3.1.2)}$$

Where, $k_j = 2\pi n/\lambda$ and d_j is the thickness of monolayer. From L_j in eqn 3.1.2, the real part of complex refraction n_j describes phase propagation and image part k_j describes light absorption.

The total transfer matrix S that relates the optical electrical field in the ambient and in the substrate is given by:

$$\begin{bmatrix} E_0^+ \\ E_0^- \end{bmatrix} = S \begin{bmatrix} E_{m+1}^+ \\ E_{m-1}^- \end{bmatrix} \text{..... (3.1.3)}$$

Where the total transfer matrix S is the product of all interfaces and layer matrices and is given by:

$$S = \begin{bmatrix} S_{11} & S_{12} \\ S_{21} & S_{22} \end{bmatrix} = \left(\prod_{v=1}^{m} I_{(v-1)v} L_v\right) I_{m(m+1)} \text{..... (3.1.4)}$$

The total optical electric field at layer j at any distance x can be expressed as:

$$E_j(x) = E_j^+(x) + E_j^-(x) \quad \text{..... (3.1.5)}$$

$E_j(x)$ can be further split into two partial transfer matrices $S_j^{'}$ and $S_j^{''}$,

$$S_j' = \begin{bmatrix} S_{j11}' & S_{j12}' \\ S_{j21}' & S_{j22}' \end{bmatrix} = \left(\prod_{v=1}^{j-1} I_{(v-1)v L_v}\right) I_{(j-1)j} \quad \ldots\ldots\ldots\ldots\ldots\ldots\ldots\ldots\ldots\ldots.. \quad (3.1.6)$$

$$S_j' = \begin{bmatrix} S_{j11}'' & S_{j12}'' \\ S_{j21}'' & S_{j22}'' \end{bmatrix} = \left(\prod_{v=j+1}^{m} I_{(v-1)v L_v}\right) I_{m(m+1)} \quad \ldots\ldots\ldots\ldots\ldots\ldots\ldots\ldots\ldots\ldots..(3.1.7)$$

The partial system transfer matrices for layer j can be determined by:

$$\begin{bmatrix} E_0^+ \\ E_0^- \end{bmatrix} = S_j' \begin{bmatrix} E_j'^+ \\ E_j'^- \end{bmatrix} \ldots\ldots\ldots\ldots\ldots\ldots\ldots\ldots\ldots\ldots\ldots\ldots\ldots\ldots\ldots\ldots\ldots\ldots\ldots\ldots\ldots\ldots(3.1.8)$$

$$\begin{bmatrix} E_j''^+ \\ E_j''^- \end{bmatrix} = S_j'' \begin{bmatrix} E_{m+1}^+ \\ E_{m-1}^- \end{bmatrix} \ldots\ldots\ldots\ldots\ldots\ldots\ldots\ldots\ldots\ldots\ldots\ldots\ldots\ldots\ldots\ldots\ldots\ldots\ldots.... \quad (3.1.9)$$

Where, $E_j'^+$ and $E_j'^-$ refer to the left boundary (j-1)j in the layer j.. $E_j''^+$ and $E_j''^-$ refer to the right boundary j(j_k+1) in layer j. Through algebraic manipulation, Eq.3.1.5 can be expresses as:

$$E_j(x) = E_j^+(x) + E_j^-(x) = t_j^+ \left[e^{ik_j x} + r_j'' e^{ik_j(2d_j - x)} \right] E_0 \quad \ldots\ldots\ldots\ldots\ldots\ldots\ldots\ldots(3.1.10)$$

Where, E_0^+ is the electric field of the incident light from the ambient.

$$t_j^+ = \left[S_{j11}' + S_{j12}' r_j'' e^{2ik_j d_j} \right]^{-1} \quad \ldots\ldots\ldots\ldots\ldots\ldots\ldots\ldots\ldots\ldots\ldots\ldots\ldots\ldots \quad (3.1.11)$$

$$r_j'' = S_{j21}'' / S_{j11}'' \quad \ldots\ldots\ldots\ldots\ldots\ldots\ldots\ldots\ldots\ldots\ldots\ldots\ldots\ldots\ldots\ldots\ldots\ldots\ldots \quad (3.1.12)$$

The light intensity at a distance x in a particular layer j can be expressed as

$$I_j(x, \boldsymbol{\lambda}) = T_j I_0(\lambda) \begin{bmatrix} e^{-\alpha_j x} + \rho_j''^2 . e^{-\alpha_j(2d_j - x)} \\ +2\rho_j'' . e^{-\alpha_j d_j} . \cos\left(\frac{4\pi n_j}{\lambda}\left(d_j - x\right) + \delta_j''\right) \end{bmatrix} \quad \ldots\ldots\ldots\ldots\ldots\ldots\ldots\ldots \quad (3.1.13)$$

In which I0(a) is the intensity of the incident light, $T_j = (\frac{n_j}{n_0}) t_j^2$ is the internal intensity transmittance, p_j'' and d_j'' are the absolute and the argument of the complex reflection

coefficient. The first term in equation 3.13 is as result of the optical electric field propagating in the positive x direction E_j^+(x), the second term is as result of the field propagating in the negative x direction E_j^-(x) and the third term is due to the optical interferences of the first two terms. The rate of energy dissipated per unit volume Q can then be determined as:

$$Q(x,\lambda) = \alpha(\lambda) I(x,\lambda) \quad \ldots\ldots\ldots\ldots\ldots\ldots\ldots\ldots\ldots\ldots\ldots\ldots\ldots\ldots\ldots\ldots\ldots\ldots \quad (3.1.14)$$

The exciton generation rate/photon absorption rate in the active layer is then given by:

$$n(x) = \int \frac{\lambda}{hc} Q(x,\lambda) d\lambda \quad \ldots\ldots\ldots\ldots\ldots\ldots\ldots\ldots\ldots\ldots\ldots\ldots\ldots\ldots\ldots\ldots\ldots\ldots \quad (3.1.15)$$

Where h is the plank constant and c is the speed of light in vacuum.

3.2 Electrical Modelling:

One dimensional drift and diffusion equations can be solved analytically to obtain the J-V characteristics of an organic bulk heterojunction solar cells [8, 25].

The Poisson's equation's is given by:

$$\frac{dF(x)}{dx} = \frac{q}{\varepsilon}[p(x) - n(x)] \quad \ldots\ldots\ldots\ldots\ldots\ldots\ldots\ldots\ldots\ldots\ldots\ldots\ldots\ldots\ldots\ldots\ldots.. \quad (3.2.1)$$

Where F is the electric field, e is the effective permittivity of the active layer composite, p(x) and n(x) are the hole and electron current density respectively,

The continuity equation for the electron and holes in steady state can be written as:

$$-\frac{1}{q}\frac{dJ_n(x)}{dx} = PG(x) - [1-P]R_L(x) \quad \ldots\ldots\ldots\ldots\ldots\ldots\ldots\ldots\ldots\ldots\ldots\ldots\ldots. \quad (3.2.2)$$

$$\frac{1}{q}\frac{dJ_p(x)}{dx} = PG(x) - [1-P]R_L(x) \ldots\ldots\ldots\ldots\ldots\ldots\ldots\ldots\ldots\ldots\ldots\ldots\ldots\ldots \quad (3.2.3)$$

Where J_n(x) and J_P(x) are the electron and hole density, P is the dissociation probability, G is the exciton generation rate and R is the bimolecular recombination. The drift and diffusion equation can be written as:

$$J_n(x) = qn(x)\mu_n F(x) + qD_n \frac{dn(x)}{dx} \quad \ldots\ldots\ldots\ldots\ldots\ldots\ldots\ldots\ldots\ldots\ldots\ldots\ldots \quad (3.2.4)$$

$$J_p(x) = qp(x)\mu_p F(x) - qD_p \frac{dp(x)}{dx} \quad \ldots\ldots\ldots\ldots\ldots\ldots\ldots\ldots\ldots\ldots\ldots\ldots\ldots(3.2.5)$$

Where μ_n and μ_P are the electron and hole mobility, D_n and D_P are the electron and hole diffusion coefficient.

The dissociation probability is determined using Onsager- Braun theory:

$$P = \frac{k_d(a,F,T)}{k_d(a,F,T)+k_f} \ldots\ldots\ldots\ldots\ldots\ldots\ldots\ldots\ldots\ldots\ldots\ldots\ldots\ldots\ldots\ldots\ldots\ldots\ldots\ldots(3.2.6)$$

Where K_d is the dissociation rate and K_f is the polaron pair decay rate.

In order to solve the drift and diffusion equation analytically following assumptions are made:

1) $F = \frac{V_a - V_{bi}}{L}$ ……………………………………………………………….(3.2.7)

2) $PG \gg (1-P)R_l$ ………………………………………………………… (3.2.8)

The first equation assumes E inside the active layer to be uniform and the second fact represent the fact that monomolecular recombination dominates bimolecular recombination. Using the drift diffusion formulization, the continuity equations can be written as

$$-\mu_n F \frac{dn}{dx} - \frac{\mu_n kT}{q}\frac{d^2n}{dx^2} = PG - (1-P)R_C \ldots\ldots\ldots\ldots\ldots\ldots\ldots\ldots\ldots\ldots\ldots\ldots\ldots \quad (3.2.9)$$

$$\mu_p F \frac{dp}{dx} - \frac{\mu_p kT}{q}\frac{d^2p}{dx^2} = PG - (1-P)R_C \ldots\ldots\ldots\ldots\ldots\ldots\ldots\ldots\ldots\ldots \quad (3.2.10)$$

The above equations can be solved using

$$n = A_n + B_n \exp\left(-\frac{qFx}{KT}\right) - \frac{PGx}{\mu_n F} + \frac{(1-P)R_C x}{\mu_n F} \ldots\ldots\ldots\ldots\ldots\ldots\ldots\ldots\ldots\ldots \quad (3.2.11)$$

$$p = A_p + B_p \exp\left(\frac{qFx}{KT}\right) - \frac{PGx}{\mu_p F} + \frac{(1-P)R_C x}{\mu_p F} \ldots\ldots\ldots\ldots\ldots\ldots\ldots\ldots\ldots\ldots \quad (3.2.12)$$

The constants A_n, B_n, A_P, B_P can determine using the boundary condition.

$$n(0) = N_C \exp\left[-\frac{(E_g - \varphi_a)}{kT}\right] \ldots\ldots\ldots\ldots\ldots\ldots\ldots\ldots\ldots\ldots\ldots\ldots\ldots\ldots \quad (3.2.13)$$

$$p(0) = N_V \exp\left[-\frac{\varphi_a}{kT}\right] \ldots\ldots\ldots\ldots\ldots\ldots\ldots\ldots\ldots\ldots\ldots\ldots\ldots\ldots\ldots\ldots \quad (3.2.14)$$

$$n(L) = N_c \exp\left[-\frac{\varphi_c}{kT}\right] \ldots\ldots\ldots\ldots\ldots\ldots\ldots\ldots\ldots\ldots\ldots\ldots\ldots\ldots\ldots\ldots \quad (3.2.15)$$

$$p(L) = N_V \exp\left[-\frac{(E_g - \varphi_c)}{kT}\right] \ldots\ldots\ldots\ldots\ldots\ldots\ldots\ldots\ldots\ldots\ldots\ldots\ldots\ldots\ldots\ldots \quad (3.2.16)$$

The obtained equation of n and p after applying the boundary condition can be used to solve J_n(x) and J_P(x). The total current density will be the sum of electron current density and hole current density.

Chapter 4

Result Analysis:

4.1 Optical Analysis of SWCNT based BHJ Solar Cell

The optical constants of the active layer materials used to determine the optical properties of the device is shown in fig 4.1 and in in fig 4.2. the optical values were extracted from [23, 24]

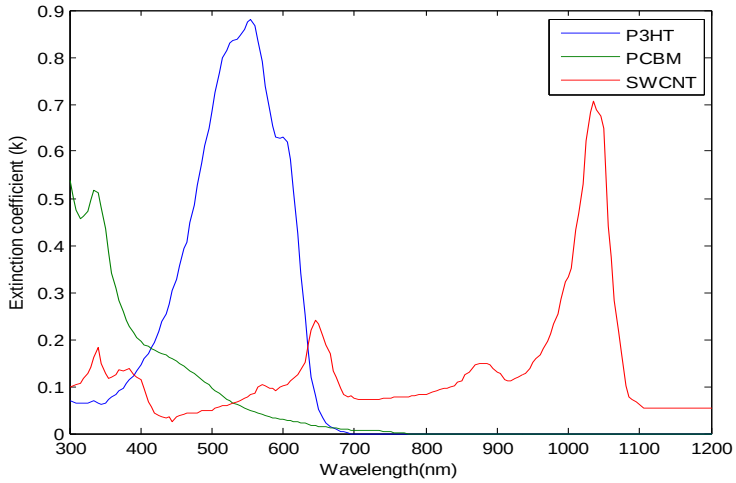

Fig 4.1: Extinction Coefficients of Active Layer Materials [23 24]

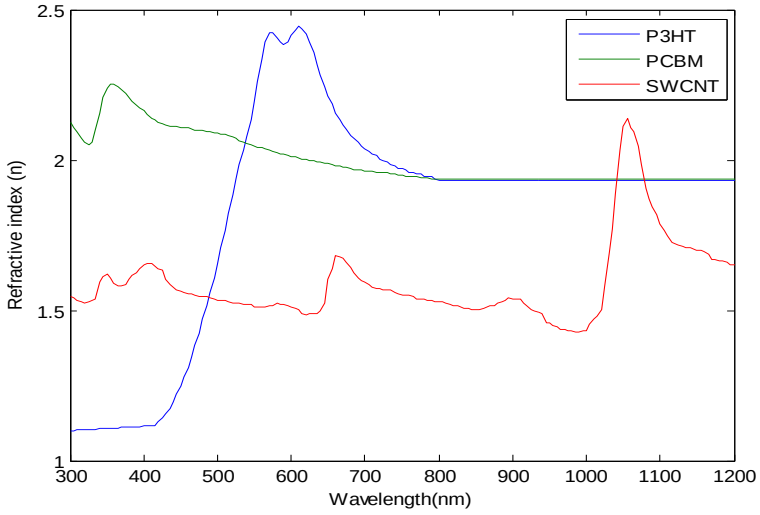

]

Fig4.2: Refractive Index of Active Layer Materials [23 24]

The absorption coefficients where determined using the extinction coefficients data shown inFig 4.1 and Fig 4.2.Fig4.3 (a) shows the absorption coefficients of a P3HT composite while Fig 4.3(b) shows the effect on the absorption coefficients after the addition of SWCNT to the mixture.What we can deduce from fig 4.3(a) is that the presense of P3HT in the the active layer composite improves the magnitude of the absorption coefficients in the UV region ranging from 450 to 650 nm. It can be seen from Fig 4.3 (b) that polymer composites consisting of SWCNTs displayed absorption coefficients in the NIR region[3]. Despite improving the the absorption coefficients in the NIR region, the presense of SWCNT could not significantly improve the absorption coefficients in the region of 300-400nm.

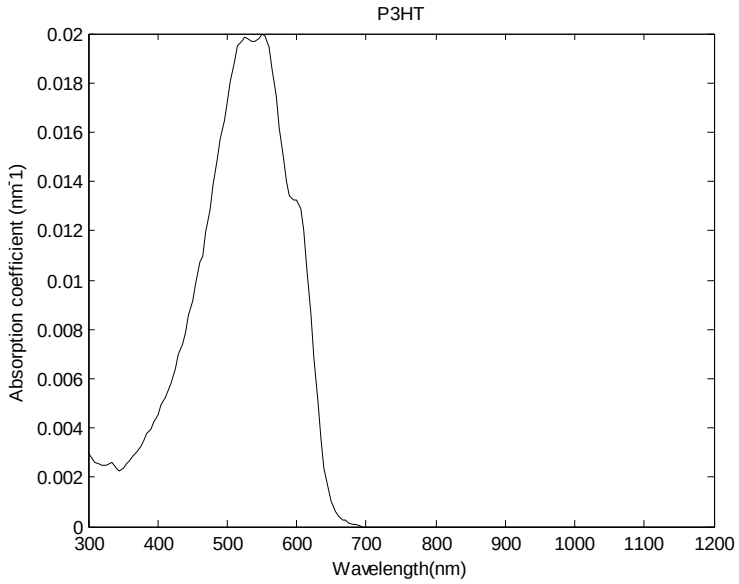

Fig 4.3 (a) Absorption Coefficinets vs Wavelength of P3HT

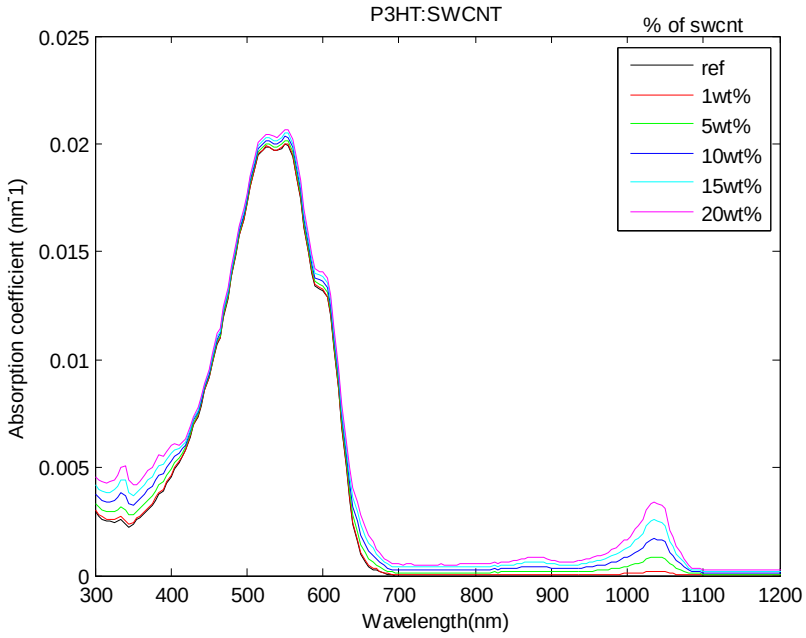

Fig 4.3 (b) Absorption Coefficinets vs Wavelength of P3HT:SWCNT

PCBM which has high extinction coefficients in the region of 300-400nm was than added to improve the overall absorption coefficient profile.Fig 4.4(a) and Fig 4.4(b) shows the predicted absorption coeffcients of P3HT:PCBM and P3HT:SWCNT:PCBM composites. As

expected the addition of PCBM to the P3HT:SWCNT composite improved the maginute of absorption coefficients in the region of 300-400nm.

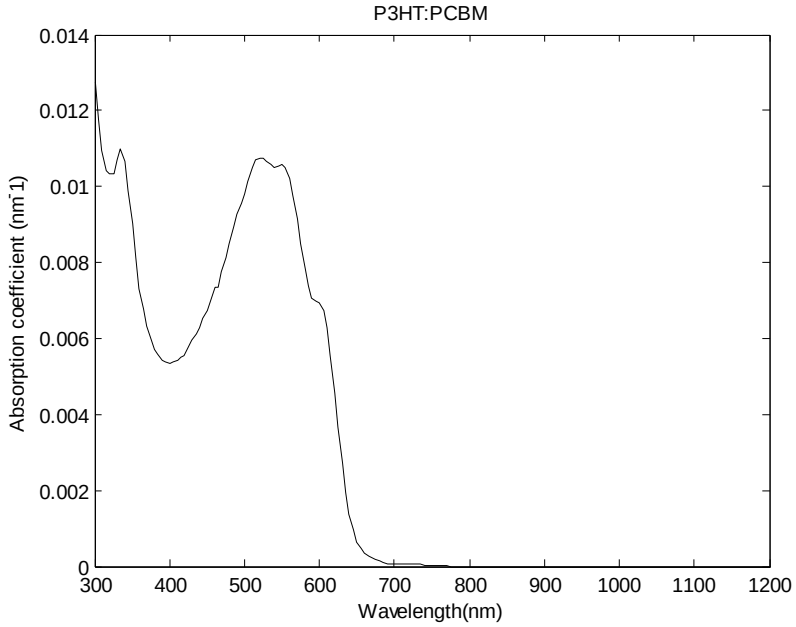

Fig 4.4 (a) Absorption Coeffiients vs Wavelength of P3HT:PCBM

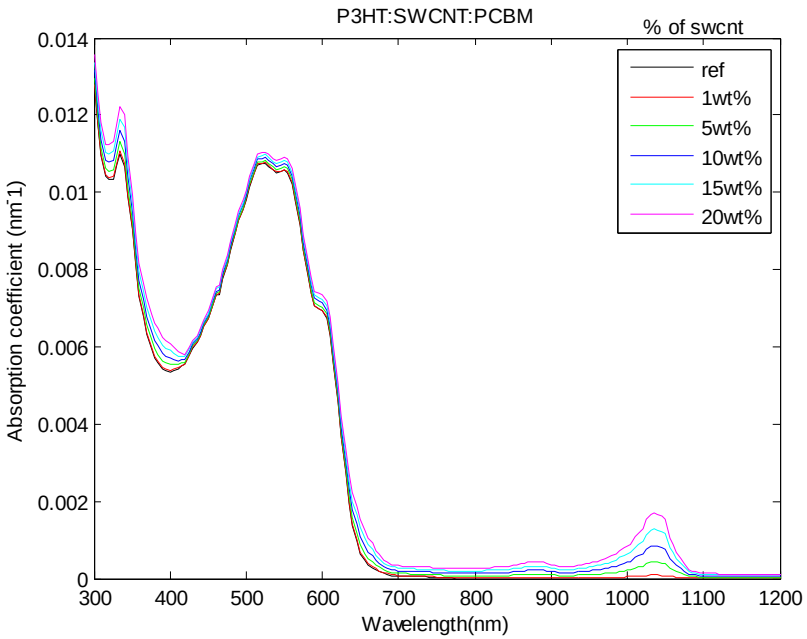

Fig 4.4 (b) Absorption Coefficinets vs Wavelength of P3HT:SWCNT:PCBM

The exciton generation rate at different active layer thickness for AM1.5G spectrum is calculated and shown in fig 4.5. Exciton generation increases with active layer thickness but shows apparent oscillation(peaks and roughs) due to the optical interface effect. The exciton generation rate for any active layer thickness increases with the additon of SWCNT. The incorporation of SWCNT resulted in the broadening of the absorption spectrum by absorbing photons with a wavelength in the NIR region.

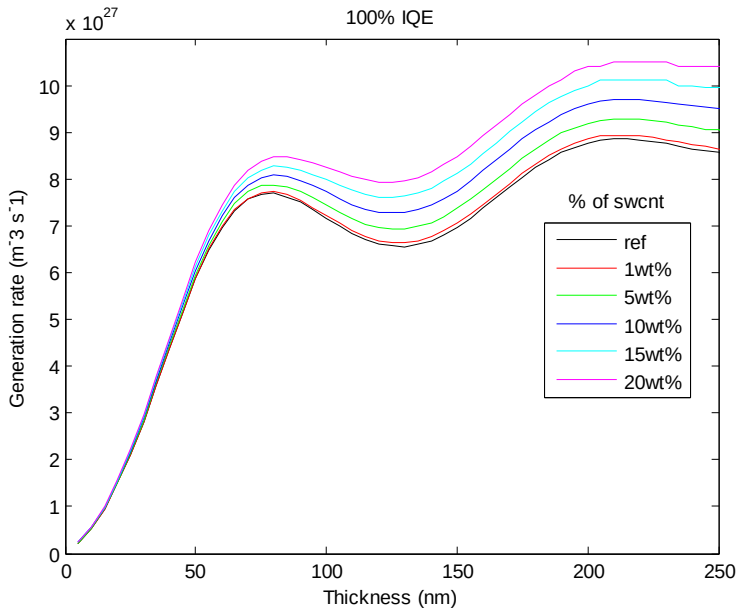

Fig 4.5: Thickness Dependent Exciton Generation Profile.

From fig 4.6 (a) it can be deduced that the incorporation SWCNT slightly enhanced the absorption in the UV region. The reference devised showed two major peaks at 340nm, 510nm and one shoulder peak at 630 nm. The addition of SWCNT increased the intensity of all the peaks achieved in the reference device. The reference device consisting of P3HT and PCBM did not show any absorbance in the NIR region. Addition of SWCNT improved that criterion by introducing a peak at 1035 nm. The peak observed at 340nm is due to the presence of PCBM in the active layer composite, while the maximum absorption peak observed at 510nm and the shoulder peak at 630nm is due the presence of P3HT in the active

layer. The peak (1035 nm) seen at the NIR region can be attributed to the second van Hove transition of s-SWCNTs. The improvement in the absorption intensity of the shoulder peak at 630 nm and at wavelengths 340 nm and 430nm can be ascribed to the first van Hove singularities of s-SWCNTs and m-SWCNTs [5].

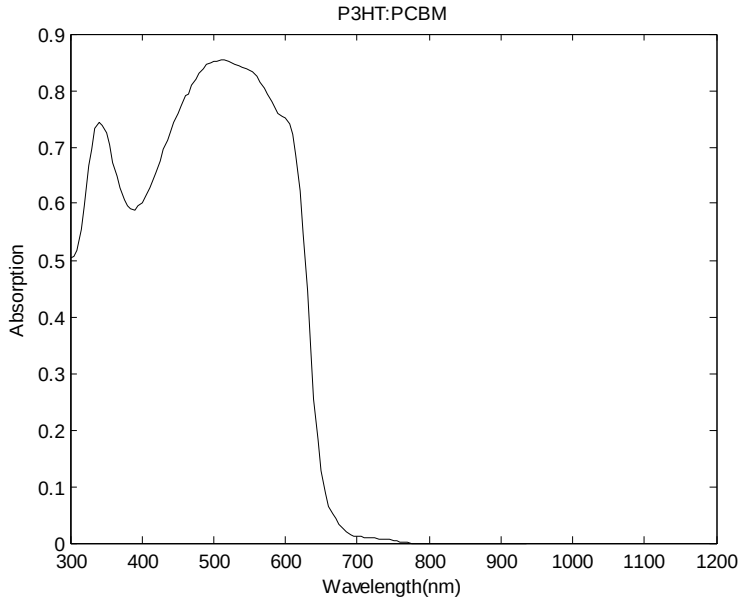

Fig 4.6 (a) Absorption Spectra vs Wavelength of P3HT:PCBM

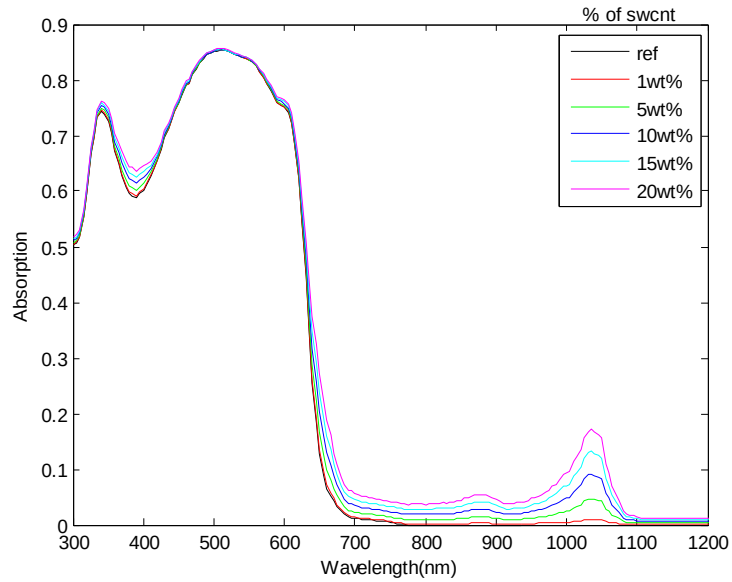

Fig 4.6(b): Absorption Spectra of P3HT: SWCNT: PCBM

From fig 4.6(b) it can be deduced that the incorporation SWCNT slightly enhanced the absorption in the UV region. The reference devised showed two major peaks at 340nm, 510nm and one shoulder peak at 630 nm. The addition of SWCNT increased the intensity of all the peaks achieved in the reference device. The reference device consisting of P3HT and PCBM did not show any absorbance in the NIR region. Addition of SWCNT improved that criterion by introducing a peak at 1035 nm.The peak observed at 340nm is due to the presence of PCBM in the active layer composite, while the maximum absorption peak observed at 510nm and the shoulder peak at 630nm is due the presence of P3HT in the active layer. The peak (1035 nm) seen at the NIR region can be attributed to the second van Hove transition of s-SWCNTs. The improvement in the absorption intensity of the shoulder peak at 630 nm and at wavelengths 340 nm and 430nm can be ascribed to the first van Hove singularities of s-SWCNTs and m-SWCNTs [5].

4.2 Electrical Analysis of SWCNT basedBHJ Solar Cells

Fig 4.7 shows the thickness dependent ehp genearation rate. In our simulation based study the major parameters affecting the net ehp generation rates are

1)carrier mobility

2)exciton binding enenrgy

3)thickness dependent exciton generation rate

4)applied elelctric Field

We have assumed that the addition of SWCNTS do not affect the overall dielctric constant of the active layer composite and hence the excition binding energy remains constant for any SWCNT based active layer composite. The applied electric field decreases with increasing thickness and since the applied electric field is a function of dissociation probability, the dissociation probability also decreases with increasing thickness. The lowering of the dissociation probability and presense low carrier mobility results in an optimized thickness of 75 nm.

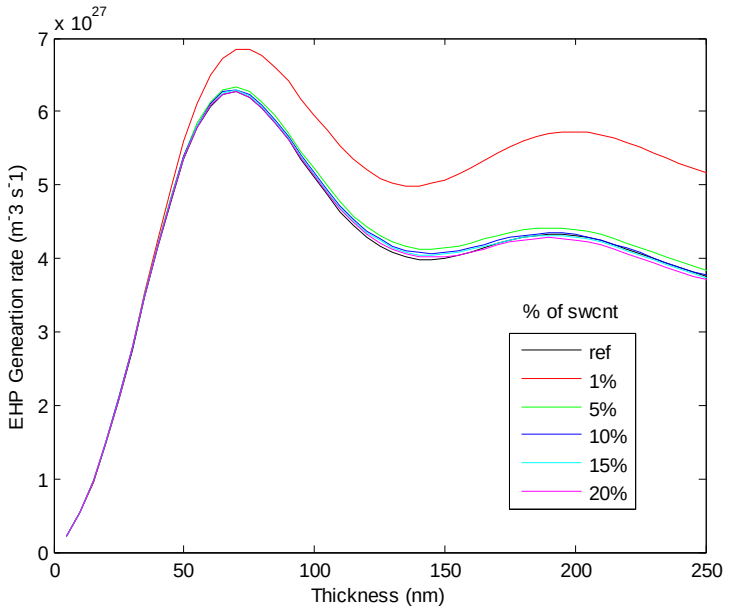

Fig 4.7: Thickness Dependent Electron Hole Pair(EHP) Generation Rate.

The highest EHP generation rate was obtained at 1wt% SWCNT and it was achieved at an optimized thickness of 75 nm. Despite of having high exciton generation rates, active layer composites with higher concentrations of SWCNT(x>5wt %) showed low EHP generation rate. For higher concentrations of SWCNTs the EHP generation rate is limited due to low carrier mobility and dissociation probability, which resulted in increased recombination loss and insufficient carrier extraction [7].

The photovoltaic performance of P3HT:SWCNT:PCBM based bulk heterojunction solar cell devices were simulated. Fig 3 shows the J-V characteristics of solar cells with varying concentration of SWCNT's. The solar cell parameters obtained from fig 4.8 is summarized in table 4.1.

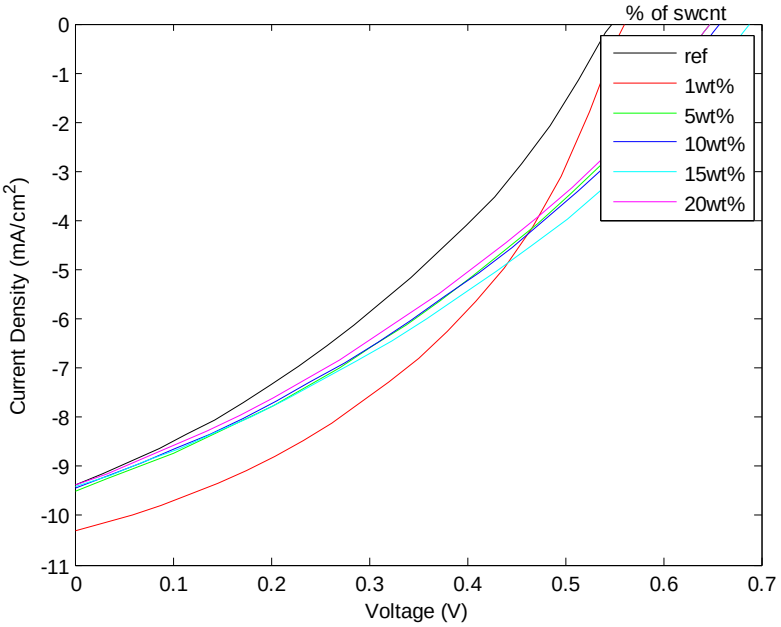

Fig 4.8: J-V Curves of P3HT:SWCNT:PCBM Based Active Layer Composites

% of SWCNT in P3HT	Jsc(mA/cm^2)	Voc(V)	FF	PCE (%)
0	9.3778	0.5476	0.345	1.7747
1	10.3149	0.56	0.4121	2.3804
5	9.4972	0.6479	0.4027	2.094
10	9.4337	0.6581	0.3372	2.0933
15	9.4091	0.6883	0.3359	2.1757
20	9.3800	0.6484	0.3345	2.0345

Table 4.1: Photovoltaic parameters of P3HT:SWCNT:PCBM solar cells

JSC:

The highest value of Jsc (10.31495mA/cm^2) was exhibited at 1 wt% SWCNT, which was effectively 10.25% greater than the Jsc (9.331mA/cm^2) of the reference device. For SWCNT concentrations greater that 1wt%, Jsc remained higher than that of the reference device but was significantly lower than that of the optimized device (1wt %).The enhancement in Jsc at low concentrations (1wt %) of SWCNT is mainly due to the increase of effective hole mobility. Enhancement hole mobility results in better conductivity and exciton dissociation probability [2,6]. The improvement in conductivity allows efficient charge transport to the cathode while an improvement in dissociation probability leads to a net increase in electron hole pair generation rate as discussed earlier.The value of Jsc at SWCNT concentrations higher than 5wt% is much lower than that of the optimized device but is higher the reference device despite having lower effective hole motilities and dissociation probabilities than the reference device. The increase of Jsc at concentrations higher than 5wt% thus could be attributed to the additional absorption of light in the NIR region (15) as shown in fig 4.6 (b).

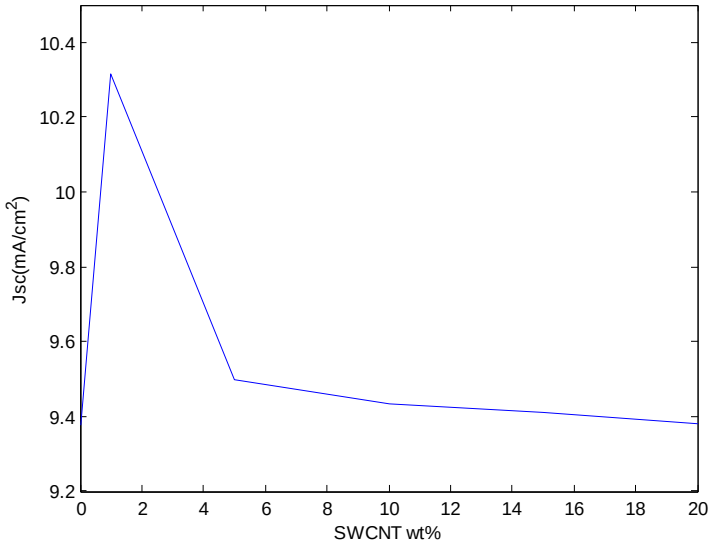

Fig 4.9: Change in Short Circuit Current Density With Increasing wt% of SWCNT

Voc:

From fig 4.9, it can be seen that there was a slight change in Voc for low concentrations of SWCNT (x<1%).The simulated Voc at 1wt% SWCNT was found to be 0.56v, which is slightly greater than the reference device (0.54V) but significant change in Voc was attained for devices with higher concentrations of SWCNT (x>5%). The highest Voc(0.688V) was obtained at 15wt% SWCNT concentration. The slight change in Voc in the optimized device in comparison to the reference device can be attributed to the fact that contribution of SWCNT at low %wt is not sufficient enough to change the HOMO and LUMO level of the active layer composite [4].Higher concentration SWCNTs(x>5wt %) resulted in high Voc. The improvement in Voc could be because of 1) a slight change in energy levels and 2) since Voc logarithmically depends on generation rate and dissociation probability, an increased Voc would also indicate that larger generation rate overcomes the effect of reduced dissociation probability. [10]

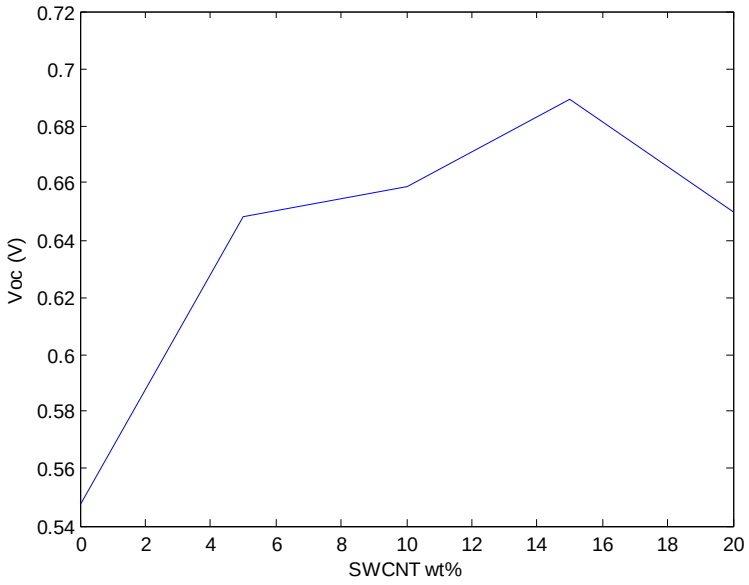

Fig 4.10: Change in Open Circuit Voltage With Increasing wt% of SWCNT

FF:

Fig 4.11 shows the change in Power conversion efficiency with increasing Highest fill factor (.4121) was achieved at 1wt% SWCNT concentration. The fill factor deteriorated with further addition of SWCNT in the active layer composite. The degree of deterioration depended on the content of SWCNT added to the active layer.FF is a function of multiple parameters thus the improvement in FF at 1wt% SWCNT cannot be attributed to a single factor. Since FF is a function of Pmax and carrier mobility, the main reasons for the improvement in FF at 1wt% SWCNT could be attributed due the improvement in Pmax and effective hole mobility. The improvement in effective hole mobility at 1wt% SWCNT has been explained earlier.

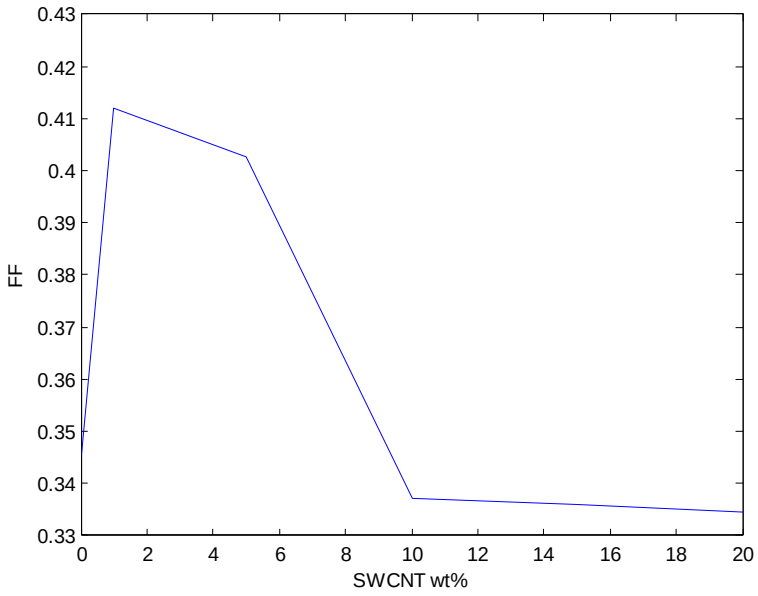

Fig 4.11: Change in Fill-Factor with Increasingwt% of SWCNT

PCE:

Fig 4.12 shows the change in Power conversion efficiency with increasing wt% of SWCNT The addition of 1wt% SWCNT to the active layer improved the PCE from 1.7789% (reference device) to 2.3804% which corresponds to a 34% enhancement in PCE, further increase in the content of SWCNT resulted in efficiencies that were greater than the reference device, but lower than the optimized device. The combined improvement in Jsc and FF ay 1wt% SWCNT resulted in an enhancement in efficiency by 34%.the reason the behind the improvement in Jsc and FF has been discussed earlier.

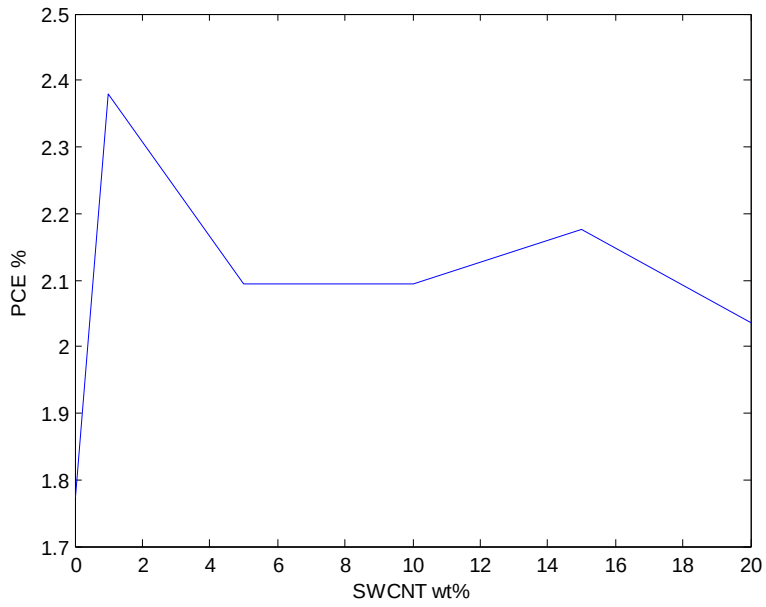

Fig 4.12: Change in Power Conversion Efficiency With Increasing wt% of SWCNT

DISCUSSION ON THE EFFECTIVE HOLE MOBILITY:

The addition of SWCNT to the reference device strongly influences the effective hole mobility of the active layer composite. The effective hole mobility data for various wt% of

SWCNTs were taken from [26, 27]. The highest hole mobility was seen at 1wt% SWCNT concentration. The hole mobility is seen to decrease for higher concentrations of SWCNT.

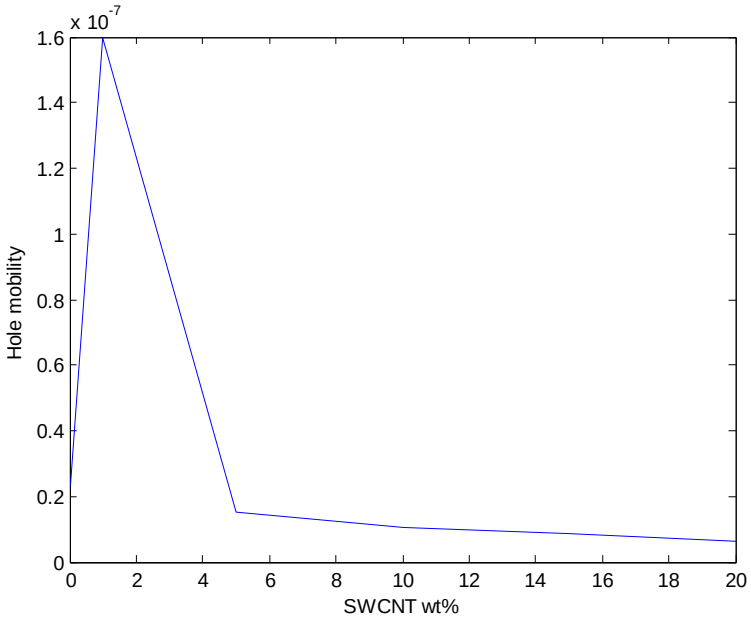

Fig 4.13: Change in Effective Hole Mobility With Increasing wt% of SWCNT [26, 27]

Increased Hole mobility and dissociation probability at 1wt% SWCNT:

The improvement in hole mobility in the presence of SWCNT could be attributed to SWCNTs 1) ballistic properties which leads to the formation of percolating pathways in the P3HT matrix. The presence of percolating pathways via nanotube leads to greater electrical conductivity leading to an efficient charge extraction out of the device through the cathode [2,3] and 2) No ground state charge transfer takes place between s-SWCNT and P3HT indicating that s-SWCNTs can form type-II heterojunction with P3HT.The formation of the type II heterojunctions leads to an increase in dissociation probability in the active layer composite [2].

Decreased hole mobility and dissociation probability for SWCNT concentration greater that 1wt%:

Despite the formation of type II junction and percolating pathways in the P3HT matrix, the hole mobility and dissociation probability of polymer composites with concentrations of SWCNT higher that 1wt% can be seen to decrease. The drastic decrease in hole mobility and dissociation probability is primarily due to the following reasons:

1) Presence of metallic SWCNTs in the Polymer: SWCNT composite. [1]

   Unlike s-SWCNTS there exists a considerable ground state charge transfer between P3HT and m-SWCNTS. This particular characteristic of m-SWCNT leads to the formation of EHP trap sites in the band gap of the P3HT: PCBM composite resulting in an increase in EHP recombination and lower effective hole mobility.

2) SWCNTs natural tendency to form aggregates of um scale

   The presence of SWCNT aggregates reduces the amount of interface available for the dissociation of excitons, the degree of aggregation tends to increase with higher content of SWCNTs and hence the exciton dissociation probability decreases with increasing SWCNT concentration. [2]

Theoretically in a mixed configuration 2/3 of the total SWCNTs are semiconducting in nature and rest 1/3 display metallic properties. For the P3HT: SWCNT interface to facilitate the exciton dissociation process, the ratio of P3HT: s-SWCNT interfaces should outweigh the ratio of P3HT: m-SWCNT .This requirement is satisfied at 1wt% SWCNT and hence an

increase is dissociation probability and hole mobility is noticed in fig 4.13, but the same principle cannot be applied for composites with higher SWCNT concentration's (x>1%), reason being that as the concentration of SWCNTs increases in the active layer composite, the majority of interfaces formed will be with m-SWCNTS because if multiple s-SWCNTS interact with one another or with m-SWCNTs they become semi-metallic in nature. The presence of m-SWCNTs as mentioned earlier results in the formation recombination centres, leading to a decrease in effective hole mobility and dissociation probability.

The effective hole mobility of a pure P3HT:s-SWCNT was predicted using the percolation theory suggested by [30]. According to theory the conductivity of a P3HT:s-SWCNT increases with SWCNT concentration. Assuming hole mobility to be proportional to conductivity, we predicted the relationship between effective hole mobility of a P3HT:s-SWCNT composite and the SWNT wt% in the P3HT matrix. Our predicted result is shown in fig 4.14

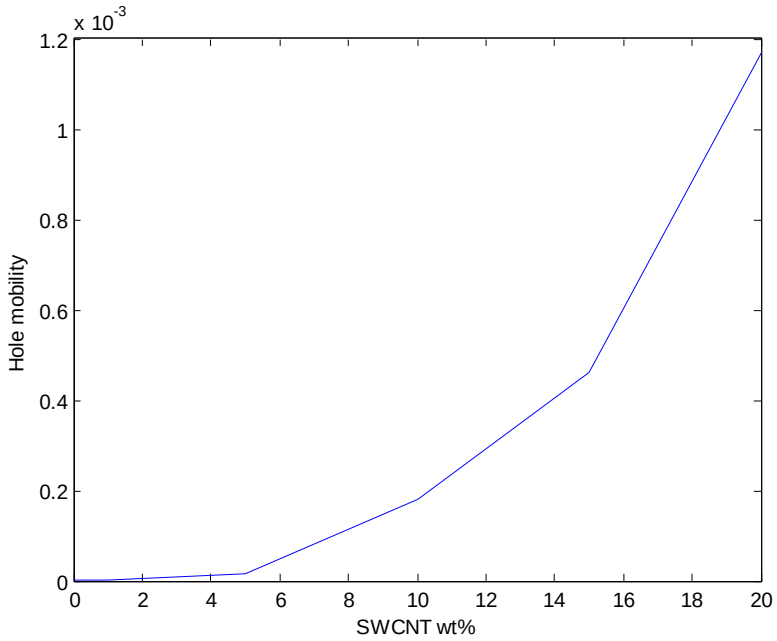

Fig 4.14: Change in Effective Hole Mobility With Increasing wt% of SWCNT

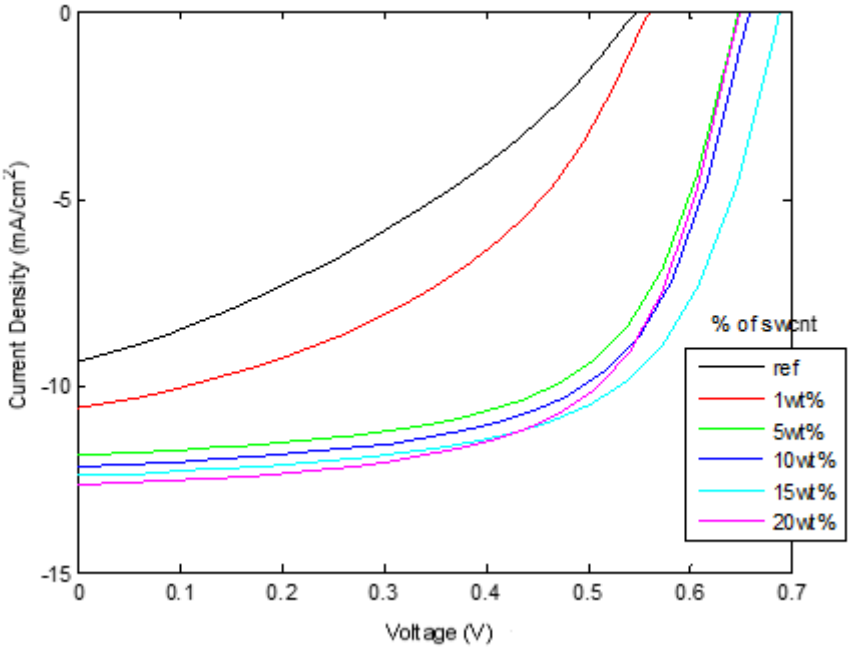

Fig 4.15: J-V Curves of P3HT:s-SWCNT:PCBM Based Active Layer Composites

% of SWCNT in P3HT	Jsc(mA/cm^2)	Voc(V)	FF	PCE (%)
0	9.3778	0.5476	0.345	1.7747
1	10.6040	0.56	0.4357	2.5870
5	11.8577	0.6479	0.6150	4,7255
10	12.1530	0.6581	0.6220	4.9749
15	12.4118	0.6883	0.6225	5.3178
20	12.6697	0.6484	0.6227	5.1151

Table 4.2: Photovoltaic Parameters of P3HT:SWCNT:PCBM Based Active Layer Composites

The highest value of Jsc (12.6697/cm^2) was exhibited at 20 wt% SWCNT, which was effectively 35.1% greater than the Jsc (9.331mA/cm^2) of the reference device. Unlike the trend shown by the impure SWCNT based BHJ, the Jsc kept on improving with increased wt% of pure s-SWCNT. This shift in trend is due to the improvement in conductivity due to percolating pathways, absorption in NIR region and due to the absence of m-SWCNTs from the active layer composites. The absence of m-SWCNTs from the mixture means that no EHP trap centres were formed to force an EHP recombination

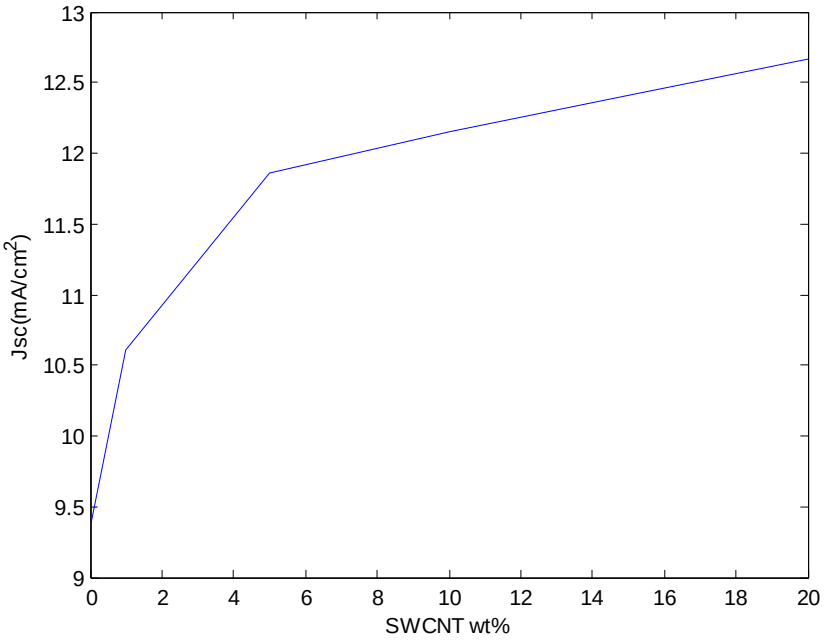

Fig 4.16: Change in Jsc with Increasingwt% of SWCNT

Voc is a function of the effective band gap and generation rate. The generation rate and effective band gap of P3HT:SWCNT:PCBM composite remains relatively the same regardless of the type of SWCNT and hence no significant change in Voc is observed

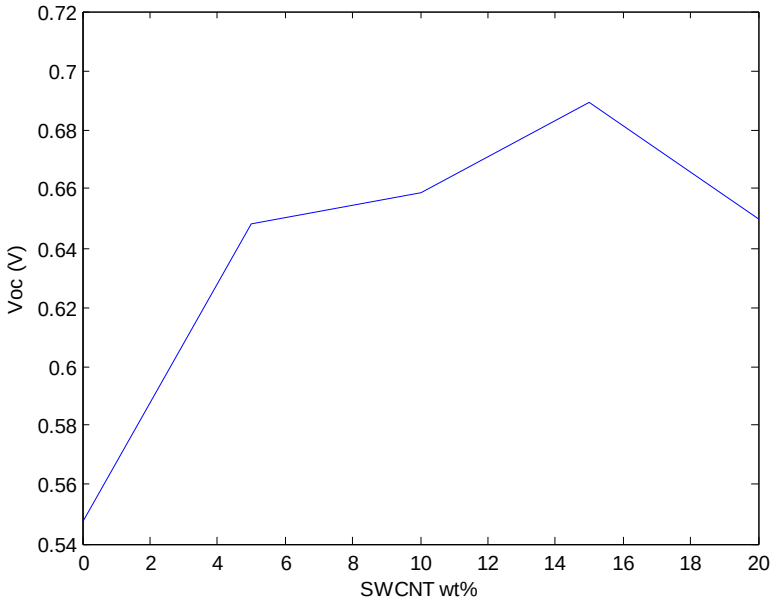

Fig 4.17: Change in Voc with Increasingwt% of SWCNT

Highest fill factor (.6227) was achieved at 20wt% SWCNT concentration. Unlike active layer composites with impure SWCNT, the fill factor of composites with pure SWCNT did not deteriorate with addition of SWCNTs greater than 1wt%. FF is a function of multiple parameters thus the improvement in FF at 20wt% SWCNT cannot be attributed to a single factor. Since FF is a function of Pmax and carrier mobility, the main reasons for the improvement in FF at 20wt% SWCNT could be attributed due the improvement in Pmax and effective hole mobility.

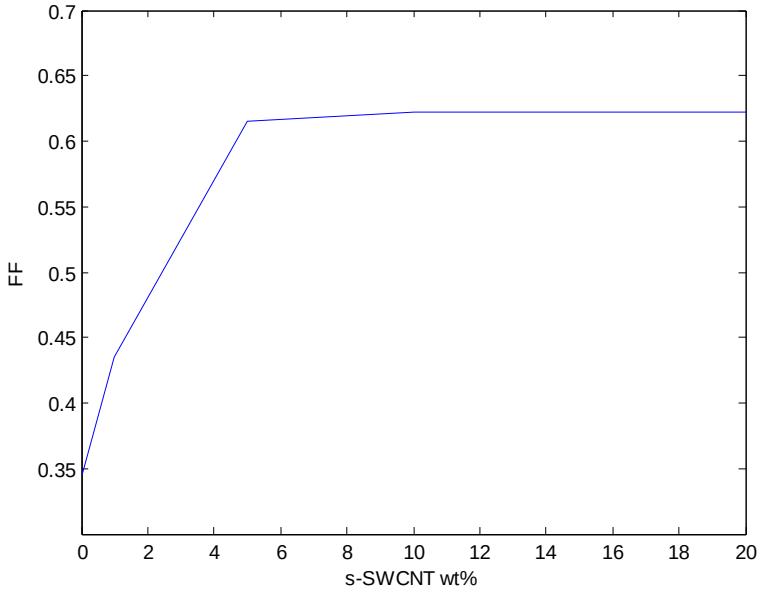

Fig 4.18: Change in FF with Increasingwt% of SWCNT

The addition of 15wt% SWCNT to the active layer improved the PCE from 1.7789% (reference device) to 5.3178% which corresponds to 200% enhancement in PCE**.** The enhancements PCE can be attributed to the improvement in Jsc and FF.

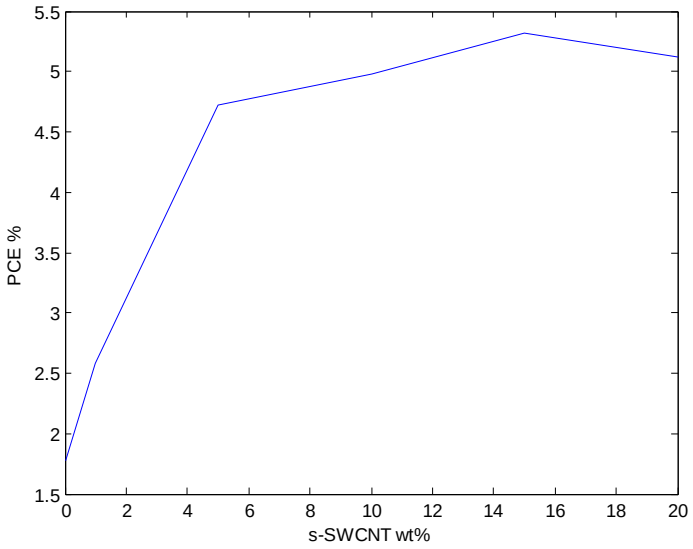

Fig 4.19: Change in Power Conversion Efficiency with Increasingwt% of SWCNT

Chapter 5

CONCLUSION AND FUTURE WORK

5.1 CONCLUSION

In conclusion the optical performance of P3HT:SWCNT:PCBM based bulk heterojunction solar cell was simulated using the optical transfer matrix methodology. The result obtained from the optical simulation show that the incorporation of SWCNT broadens of the absorption spectrum by absorbing photons with a wavelength in the NIR region. Although the position of the absorption peaks in the absorbance spectrum do not get shifted with the addition of SWCNT, the intensity of the absorption peaks does increase with added content of SWCNT. To simulate the JV characteristics of the SWCNT based devices, one dimensional drift diffusion equations were solved analytically. The reference solar cell device with an active layer composed of P3HT:PCBM was found to have a short current density (Jsc) of 9.3778 mA, an open circuit voltage (Voc) of 0.547V and a fill factor (FF) of 0.345 leading to a PCE of 1.7747%. The highest PCE was achieved through the incorporation at 1wt% SWCNT. Upon the addition of 1wt% SWCNT the Jsc, Voc and FF enhanced to 10.3144mA, 0.56V and 0.4121 leading to an improved PCE of 2.38%. Incorporation of SWCNTs above 1% resulted decreased the PCE. J-V analysis revealed that the solar cell parameters limiting the PCE at higher wt% of SWCNT was the FF and Jsc. From our theoretical analysis we found that the decrease in Jsc and FF for higher wt% of SWCNT was due the decrease in effective hole mobility at higher concentrations of SWCNT. The decrease in effective hole mobility was attributed to the presence of m-SWCNT which made a pathway for EHP recombination and SWCNT aggregation which decreased the dissociation

probability. We then predicted the J-V characteristics of 75 nm thick P3HT: SWCNT: PCBM based bulk hetero junction solar cells by considering s-SWCNTs without any impurities. The highest PCE (5.1378%) was achieved by incorporating pure 15wt% s-SWCNT. The result shows thata pure s-SWCNT has the capability to enhance the PCE of a P3HT: PCBM based bulk heterojunction solar cell by 200%.

5.2 FUTURE WORK

Further improvement in the PCE of a BHJ solar cell could be achieved by simulating the effect of adding :

- Low band gap polymer (PTB7) with greater hole carrier mobility
- Higher absorbing PC70BM with greater electron mobility
- Hole Transport Layer
- s-SWCNTS of different chiralities and diameter

Bibliography

[1]A. Mallajosyula, S. Sundar Kumar Iyer and B. Mazhari, "Increasing the efficiency of charge extraction limited poly-(3-hexylthiophene):[6,6] phenyl C61 butyric acid methyl ester solar cells using single walled carbon nanotubes with metallic characteristics", *J. Appl. Phys.*, vol. 109, no. 12, p. 124908, 2011.

[2]S. Ren, M. Bernardi, R. Lunt, V. Bulovic, J. Grossman and S. GradeÄ • ak, "Toward Efficient Carbon Nanotube/P3HT Solar Cells: Active Layer Morphology, Electrical, and Optical Properties", *Nano Letters*, vol. 11, no. 12, pp. 5316-5321, 2011.

[3]G. Jun, S. Jin, S. Park, S. Jeon and S. Hong, "Highly dispersed carbon nanotubes in organic media for polymer:fullerene photovoltaic devices", *Carbon*, vol. 50, no. 1, pp. 40-46, 2012.

[4]L. Koster, V. Mihailetchi, R. Ramaker and P. Blom, "Light intensity dependence of open-circuit voltage of polymer:fullerene solar cells", *Appl. Phys. Lett.*, vol. 86, no. 12, p. 123509, 2005.

[5]S. Cataldo, P. Salice, E. Menna and B. Pignataro, "Carbon nanotubes and organic solar cells", *Energy Environ. Sci.*, vol. 5, no. 3, pp. 5919-5940, 2012.

[6]J. Arranz-AndrÃ©s and W. Blau, "Enhanced device performance using different carbon nanotube types in polymer photovoltaic devices", *Carbon*, vol. 46, no. 15, pp. 2067-2075, 2008.

[7]L. Pettersson, L. Roman and O. InganaÌˆs, "Modeling photocurrent action spectra of photovoltaic devices based on organic thin films", *J. Appl. Phys.*, vol. 86, no. 1, p. 487, 1999.

[8]M. Inche Ibrahim, Z. Ahmad and K. Sulaiman, "Analytical expression for the current-voltage characteristics of organic bulk heterojunction solar cells", *AIP Advances*, vol. 5, no. 2, p. 027115, 2015.

[9]J. Lee, J. Lim, N. Lee, H. Park, K. Lee, T. Jeon, S. Nam, J. Kim, J. Shin and S. Kim, "Synergistic Concurrent Enhancement of Charge Generation, Dissociation, and Transport in Organic Solar Cells with Plasmonic Metal-Carbon Nanotube Hybrids", *Adv. Mater.*, vol. 27, no. 9, pp. 1519-1525, 2014.

[10]L. Lu, T. Xu, W. Chen, J. Lee, Z. Luo, I. Jung, H. Park, S. Kim and L. Yu, "The Role of N-Doped Multiwall Carbon Nanotubes in Achieving Highly Efficient Polymer Bulk Heterojunction Solar Cells", *Nano Letters*, vol. 13, no. 6, pp. 2365-2369, 2013.

[11]J. Lee, J. Park, S. Lee, H. Kim, S. Yoo and S. Kim, "Selective Electron- or Hole-Transport Enhancement in Bulk-Heterojunction Organic Solar Cells with N- or B-Doped Carbon Nanotubes", *Adv. Mater.*, vol. 23, no. 5, pp. 629-633, 2010.

[12]G. Dabera, K. Jayawardena, M. Prabhath, I. Yahya, Y. Tan, N. Nismy, H. Shiozawa, M. Sauer, G. Ruiz-Soria, P. Ayala, V. Stolojan, A. Adikaari, P. Jarowski, T. Pichler and S. Silva, "Hybrid Carbon Nanotube Networks as Efficient Hole Extraction Layers for Organic Photovoltaics", *ACS Nano*, vol. 7, no. 1, pp. 556-565, 2013.

[13]J. Lee, B. Kwon, H. Park, H. Kim, M. Kim, J. Park, E. Kim, S. Yoo, D. Jeon and S. Kim, "Exciton Dissociation and Charge-Transport Enhancement in Organic Solar Cells with Quantum-Dot/N-doped CNT Hybrid Nanomaterials", *Adv. Mater.*, vol. 25, no. 14, pp. 2011-2017, 2013.

[15]Brabec CJ, Sariciftci NS, Hummelen JC (2001) Plastic solar cells. origin of the open circuit

voltage of plastic solar cells. Adv Funct Mater 11:15–26. doi:1616-301X/01/0510-0379

[16]Scharber MC, Wuhlbacher D, Koppe M (2006) Design rules for donors bulkheterojunction solar cells—towards 10% energy-conversion efficiency. Adv Mater 18:789–

794. doi:10.1002/adma.200501717

[17] Sariciftci NS, Braun D, Zhang C, Srdanov VI, Heeger AJ, Stucky G, Wudl F (1993) Semiconducting polymerbuckminsterfullerene heterojunctions: diodes, photodiodes, and photovoltaic cells. Appl Phys Lett 62:585–587. doi:10.1063/1.108863

[18] He YJ, Li YF (2011) Fullerene derivative acceptors for high performance polymer solar cells Phys Chem Chem Phys 13:1970–1983. doi:10.1021/ja103275u

[19] Lenes M, Shelton SW, Sieval AB, Kronholm DF, Hummelen JC, Blom PWM (2009) Electron trapping in higher adduct fullerene-based solar cells. Adv Funct Mater 19:3002–3007. doi:10.1002/adfm.200900459

[20] Shaheen S. Ginley, D. Jabbour G., "Organic-Based Photovoltaics: Towards Low-Cost Power Generation" *MRS Bulletin* **30**, 10-15, 2005.

[21] Hoppe, Sariciftci. "Organic Solar Cells: An Overview" *J. Mat. Res.* **19** (7) 1924-45, 2004**.**

[22] Sariciftci et al. "Polymer–Fullerene Bulk Heterojunction Solar Cells." *MRS Bulletin* **30**, 33-6, 2005.

[23] Lenes M, Wetzelaer G, Kooist FB, Veenstra SJJC, Blom PWM (2008) Fullerene bisadducts

for enhanced open-circuit voltages and efficiencies in polymer solar cells. Adv Mater 20:2116–2119. doi:10.1002/adma.200702438

[23]Guillot, Sarah L. et al. "Precision Printing And Optical Modeling Of Ultrathin SWCNT/C 60 Heterojunction Solar Cells". *Nanoscale* 7.15 (2015): 6556-6566. Web. 17 Dec. 2015.

[24]Web.stanford.edu,. "Mcgehee Group - Stanford Materials Science And Engineering". N.p., 2015. Web. 17 Dec. 2015.

[26]Lee, Ju Min et al. "Selective Electron- Or Hole-Transport Enhancement In Bulk-Heterojunction Organic Solar Cells With N- Or B-Doped Carbon Nanotubes". *Adv. Mater.* 23.5 (2010): 629-633. Web. 18 Dec. 2015.

[27]Rudenko, Andrey E., Petr P. Khlyabich, and Barry C. Thompson. "Random Poly(3-Hexylthiophene- Co -3-Cyanothiophene) Copolymers Via Direct Arylation Polymerization (Darp) For Organic Solar Cells With High Open-Circuit Voltage". *ACS Macro Lett.* 3.4 (2014): 387-392. Web. 18 Dec. 2015.

[28]G. Cakmak, H. Guney, S. Aydın Yuksel and S. Gunes, "The effect of functionalized single walled carbon nanotube with octadecylamine on efficiency of poly-(3-hexylthiophene): [(6,6)] phenyl C61 butyric acid methyl ester organic solar cells", *Physica B: Condensed Matter*, vol. 461, pp. 85-91, 2015.

[29]A. Mallajosyula, S. Iyer and B. Mazhari, "Role of single walled carbon nanotubes in improving the efficiency of poly-(3-hexylthiophene) based organic solar cells", *J. Appl. Phys.*, vol. 108, no. 9, p. 094902, 2010.

[30] I. Singh, P. Bhatnagar, P. Mathur, I. Kaur, L. Bharadwaj and R. Pandey, "Optical and electrical characterization of conducting polymer-single walled carbon nanotube composite films", *Carbon*, vol. 46, no. 8, pp. 1141-1144, 2008.

[31]F. Krebs, T. Tromholt and M. Jørgensen, "Upscaling of polymer solar cell fabrication using full roll-to-roll processing", *Nanoscale*, vol. 2, no. 6, p. 873, 2010.

[32]Google.com,2015.[Online].Available:https://www.google.com/url?sa=t&rct=j&q=&esrc=s&source=web&cd=1&cad=rja&uact=8&ved=0ahUKEwja9N7KxOXJAhUGHI4KHQ-TDLsQFgglMAA&url=http%3A%2F%2Fwww.springer.com%2Fcda%2Fcontent%2Fdocument%2Fcda_downloaddocument%2F9781447148227-c2.pdf%3FSGWID%3D0-0-45-1367021-p174705574&usg=AFQjCNHuooYB3zsJE7liP-3RPr5W8uPncQ&sig2=CyHfII0DUP5HiKZQg7BpAA. [Accessed: 18- Dec- 2015]

[33] T.Grace, "An Introduction to Carbon Nanotubes," summer, Stanford University, 2003.

[34] Xiaolei Liu, "Synthesis, Devices and Applications of Carbon Nanotubes," Thesis report, University of Southern California, January 2006

SIMULATION CODES:

OPTICAL MODELLING:

```
functionTransferMatrix
%------------BEGIN USER INPUT PARAMETERS SPECITIFCATION-------
--------
%
lambda=300:5:1700; % Wavelengths over which field patterns are
calculated
stepsize = 1;   % The electric field is calculated at a latice
of points (nm)
% in the device cross section seperated by this distance

% plotWavelengths specifies which wavelengths to plot when
plotting E-field
% intensity distributions (figure 1). Specify values by adding
wavelength
% values to the array. Values must be within the range of
calculated
% wavelenths (ie. must be an element of the lambda array). All
wavelengths
% are in nanometers.
plotWavelengths = [370 380 390];

% Specify Layers in device (an arbitrary number of layers is
permitted) and
% thicknesses.
%
% Change these arrays to change the order or number of layers
and/or
% thickness of layers. List the layers in the order that they
appear in the
% device starting with the side the light is incident on.  THE
NAMES OF THE
% LAYERS MUST CORRESPOND TO THE NAMES OF THE MATERIALS IN THE
INDEX OF
% REFRACTION LIBRARY FILE, 'Index_of_Refraction_library.xls'.
The first
% layer must be the transparent substrate (glass) or 'Air' if
the active
% layers are on the reflective electrode (rather than
transparent electrode) side
% of the device.  The layer thicknesses are in nanometers.

layers = {'SiO2''ITOsorizon''PEDOT''k20''Ca''Al'}; % Names of
layers of materials starting from side light is incident from
```

```
thicknesses = [0 100 25 75 7 100];  % thickness of each
corresponding layer in nm (thickness of the first layer is
irrelivant)

% Set plotGeneration to 'true' if you want to plot generation
rate as a
% function of position in the device and output the calculated
short circuit current
% under AM1.5G illumination (assuming 100% internal quantum
efficiency)
plotGeneration = true;
activeLayer = 4; % index of material layer where photocurrent
is generated
%
%------------END USER INPUT PARAMETERS SPECIFICATION----------
---------



% Load in index of refraction for each material
n = zeros(size(layers,2),size(lambda,2));
for index = 1:size(layers,2)
n(index,:) = LoadRefrIndex(layers{index},lambda);
end
t = thicknesses;

% Constants
h = 6.62606957e-34;     % Js Planck's constant
c = 2.99792458e8;   % m/s speed of light
q = 1.60217657e-19; % C electric charge

% Calculate Incoherent power transmission through substrate
% See Griffiths "Intro to Electrodynamics 3rd Ed. Eq. 9.86 &
9.87
T_glass=abs(4*1*n(1,:)./(1+n(1,:)).^2);
R_glass=abs((1-n(1,:))./(1+n(1,:))).^2;

% Calculate transfer matrices, and field at each wavelength
and position
t(1)=0;
t_cumsum=cumsum(t);
x_pos=(stepsize/2):stepsize:sum(t); %positions to evaluate
field
%x_mat specifies what layer number the corresponding point in
x_pos is in:
x_mat=
sum(repmat(x_pos,length(t),1)>repmat(t_cumsum',1,length(x_pos)
),1)+1;
R=lambda*0;
E=zeros(length(x_pos),length(lambda));
for l = 1:length(lambda)
```

```
% Calculate transfer matrices for incoherent reflection and
transmission at the first interface
    S=I_mat(n(1,l),n(2,l));
formatindex=2:(length(t)-1)

S=S*L_mat(n(matindex,l),t(matindex),lambda(l))*I_mat(n(matinde
x,l),n(matindex+1,l));
end
R(l)=abs(S(2,1)/S(1,1))^2; %JAP Vol 86 p.487 Eq 9 Power
Reflection from layers other than substrate
T(l)=abs(2/(1+n(1,l)))/sqrt(1-R_glass(l)*R(l)); %Transmission
of field through glass substrate Griffiths 9.85 + multiple
reflection geometric series

% Calculate all other transfer matrices
for material = 2:length(t)
xi=2*pi*n(material,l)/lambda(l);
dj=t(material);
x_indices=find(x_mat == material); %indices of points which
are in the material layer considered
        x=x_pos(x_indices)-t_cumsum(material-1); %distance
from interface with previous layer
% Calculate S matrices (JAP Vol 86 p.487 Eq 12 and 13)
S_prime=I_mat(n(1,l),n(2,l));
formatindex=3:material
            S_prime=S_prime*L_mat(n(matindex-1,l),t(matindex-
1),lambda(l))*I_mat(n(matindex-1,l),n(matindex,l));
end
S_doubleprime=eye(2);
formatindex=material:(length(t)-1)

S_doubleprime=S_doubleprime*I_mat(n(matindex,l),n(matindex+1,l
))*L_mat(n(matindex+1,l),t(matindex+1),lambda(l));
end
% Normalized Field profile (JAP Vol 86 p.487 Eq 22)
        E(x_indices,l)=T(l)*(S_doubleprime(1,1)*exp(-
1i*xi*(dj-x))+S_doubleprime(2,1)*exp(1i*xi*(dj-x)))
./(S_prime(1,1)*S_doubleprime(1,1)*exp(-
1i*xi*dj)+S_prime(1,2)*S_doubleprime(2,1)*exp(1i*xi*dj));
end
end

% Overall Reflection from device with incoherent reflections
at first
% interface (typically air-glass)
Reflection=R_glass+T_glass.^2.*R./(1-R_glass.*R);

% Plots electric field intensity |E|^2 vs position in device
for
% wavelengths specified in the initial array, plotWavelengths.
closeall
```

```
figure(1)
plotString = '';
legendString = cell(1,size(plotWavelengths,2));
for index=1:size(plotWavelengths,2)
plotString = strcat(plotString, ['x_pos,abs(E(:,',
num2str(find(lambda == plotWavelengths(index))), ').^2),']);
legendString{index} = [num2str(plotWavelengths(index)), '
nm'];
end
eval(['plot(', plotString, '''LineWidth'',2)'])
axislimit1=axis;

% Draws vertical lines at each material boundary in the stack
and labels
% each layer
formatindex=2:length(t)
    line([sum(t(1:matindex)) sum(t(1:matindex))],[0
axislimit1(4)]);
text((t_cumsum(matindex)+t_cumsum(matindex-
1))/2,0,layers{matindex},'HorizontalAlignment','center','Verti
calAlignment','bottom')
end

title('E-field instensity in device');
xlabel('Position in Device (nm)');
ylabel('Normalized Electric field intensity |E|^2');
legend(legendString);

% Absorption coefficient in cm^-1 (JAP Vol 86 p.487 Eq 23)
a=zeros(length(t),length(lambda));
formatindex=2:length(t)
a(matindex,:)=4*pi*imag(n(matindex,:))./(lambda*1e-7);
end

% Plots normalized intensity absorbed /cm3-nm at each position
and
% wavelength as well as the total reflection expected from the
device
% (useful for comparing with experimentally measured
reflection spectrum)
figure(2)
Absorption=zeros(length(t),length(lambda));
plotString = '';
formatindex=2:length(t)
Pos=find(x_mat == matindex);

AbsRate=repmat(a(matindex,:).*real(n(matindex,:)),length(Pos),
1).*(abs(E(Pos,:)).^2);
Absorption(matindex,:)=sum(AbsRate,1)*stepsize*1e-7;
plotString = strcat(plotString, ['lambda,Absorption(',
num2str(matindex), ',:),']);
```

```
end

eval(['plot(', plotString,
'lambda,Reflection,''LineWidth'',2)'])
title('Fraction of Light absorbed or reflected');
xlabel('Wavelength (nm)');
ylabel('Light Intensity Fraction');
legend(layers{2:size(layers,2)}, 'Reflectance');

% Plots generation rate as a function of position in the
device and
% calculates Jsc
ifplotGeneration == true

% Load in 1sun AM 1.5 solar spectrum in mW/cm2nm
    AM15_data=xlsread('AM15.xls');
    AM15=interp1(AM15_data(:,1), AM15_data(:,2), lambda,
'linear', 'extrap');

figure(3)
% Energy dissipation mW/cm3-nm at each position and wavelength
(JAP Vol
% 86 p.487 Eq 22)
ActivePos=find(x_mat == activeLayer);

Q=repmat(a(activeLayer,:).*real(n(activeLayer,:)).*AM15,length
(ActivePos),1).*(abs(E(ActivePos,:)).^2);

% Exciton generation rate per second-cm3-nm at each position
and wavelength
Gxl=(Q*1e-3).*repmat(lambda*1e-9,length(ActivePos),1)/(h*c);

if length(lambda)==1
lambdastep= 1;
else
lambdastep=(max(lambda)-min(lambda))/(length(lambda)-1);
end
Gx=sum(Gxl,2)*lambdastep; % Exciton generation rate as a
function of position/(sec-cm^3)
plot(x_pos(ActivePos),Gx,'LineWidth',2)
    axislimit3=axis;
axis([axislimit1(1:2) axislimit3(3:4)])
% inserts vertical lines at material boundaries
formatindex=2:length(t)
        line([sum(t(1:matindex)) sum(t(1:matindex))],[0
axislimit3(4)]);
text((t_cumsum(matindex)+t_cumsum(matindex-
1))/2,0,layers{matindex},'HorizontalAlignment','center','Verti
calAlignment','bottom')
end
```

```
title('Generation Rate in Device')
xlabel('Position in Device (nm)');
ylabel('Generation rate /(sec-cm^3)');

% outputs predicted Jsc under AM1.5 illumination assuming 100%
internal
% quantum efficiency at all wavelengths
Jsc=sum(Gx)*stepsize*1e-7*q*1e3 %in mA/cm^2

% Calculate parasitic absorption
parasitic_abs=(1-Reflection-Absorption(activeLayer,:))';

% sends absorption, reflection, and wavelength data to the
workspace
assignin('base','absorption',Absorption');
assignin('base','reflection',Reflection');
assignin('base','parasitic_abs',parasitic_abs);
assignin('base','lambda',lambda');
end

%------------------- Helper Functions ----------------------
------------
% Function I_mat
% This function calculates the transfer matrix, I, for
reflection and
% transmission at an interface between materials with complex
dielectric
% constant n1 and n2.
function I = I_mat(n1,n2)
r=(n1-n2)/(n1+n2);
t=2*n1/(n1+n2);
I=[1 r; r 1]/t;

% Function L_mat
% This function calculates the propagation matrix, L, through
a material of
% complex dielectric constant n and thickness d for the
wavelength lambda.
function L = L_mat(n,d,lambda)
xi=2*pi*n/lambda;
L=[exp(-1i*xi*d) 0; 0 exp(1i*xi*d)];

% Function LoadRefrIndex
% This function returns the complex index of refraction
spectra, ntotal, for the
% material called 'name' for each wavelength value in the
wavelength vector
% 'wavelengths'.  The material must be present in the index of
refraction
% library 'Index_of_Refraction_library.xls'.  The program uses
linear
```

```
% interpolation/extrapolation to determine the index of
refraction for
% wavelengths not listed in the library.
functionntotal = LoadRefrIndex(name,wavelengths)

%Data in IndRefr, Column names in IndRefr_names
[IndRefr,IndRefr_names]=xlsread('Indeex_of_Refraction_library.
xls');

% Load index of refraction data in spread sheet, will crash if
misspelled
file_wavelengths=IndRefr(:,strmatch('Wavelength',IndRefr_names
));
n=IndRefr(:,strmatch(strcat(name,'_n'),IndRefr_names));
k=IndRefr(:,strmatch(strcat(name,'_k'),IndRefr_names));

% Interpolate/Extrapolate data linearly to desired wavelengths
n_interp=interp1(file_wavelengths, n, wavelengths, 'linear',
'extrap');
k_interp=interp1(file_wavelengths, k, wavelengths, 'linear',
'extrap');

%Return interpolated complex index of refraction data
ntotal = n_interp+1i*k_interp;
```

THICKNESS DEPENDENT GENERATION PROFILE:

```
functionTransferMatrix_VaryThickness
%------------BEGIN USER INPUT PARAMETERS SPECITIFCATION-------
--------
%
lambda=300:5:1700; % Wavelengths over which field patterns are
calculated
stepsize = 1;   % The electric field is calculated at a latice
of points (nm)
% in the device cross section seperated by this distance

% Specify Layers in device (an arbitrary number of layers is
permitted) and
% thicknesses.
%
% Change these arrays to change the order or number of layers
and/or
% thickness of layers. List the layers in the order that they
appear in the
% device starting with the side the light is incident on.  THE
NAMES OF THE
% LAYERS MUST CORRESPOND TO THE NAMES OF THE MATERIALS IN THE
INDEX OF
% REFRACTION LIBRARY FILE, 'Index_of_Refraction_library.xls'.
The first
% layer must be the transparent substrate (glass) or 'Air' if
the active
% layers are on the reflective electrode (rather than
transparent electrode) side
% of the device.  The layer thicknesses are in nanometers.

layers = {'SiO2''ITOsorizon''PEDOT''PTB7''Ca''Al'}; % Names of
layers of materials starting from side light is incident from
thicknesses = [0 100 25 100 7 200];  % thickness of each
corresponding layer in nm (thickness of the first layer, and
layer which thickness is varied is irrelivant)

% Set plotGeneration to 'true' if you want to plot generation
rate as a
% function of position in the device and output the calculated
short circuit current
% under AM1.5G illumination (assuming 100% internal quantum
efficiency)
% plotGeneration = true;
activeLayer = 4; % index of material layer where photocurrent
is generated
LayerVaried = 4; % index of material where thickness will be
varied
VaryThickness = 5:5:300; % thickness values for layer that
will be varied in thickness in nm
```

```
%
%------------END USER INPUT PARAMETERS SPECIFICATION----------
---------

% Load in 1sun AM 1.5 solar spectrum in mW/cm2nm
AM15_data=xlsread('AM15.xls');
AM15=interp1(AM15_data(:,1), AM15_data(:,2), lambda, 'linear',
'extrap');

% Load in index of refraction for each material
n = zeros(size(layers,2),size(lambda,2));
for index = 1:size(layers,2)
n(index,:) = LoadRefrIndex(layers{index},lambda);
end

% Constants
h = 6.62606957e-34;     % Js Planck's constant
c = 2.99792458e8;   % m/s speed of light
q = 1.60217657e-19; % C electric charge

% Calculate Incoherent power transmission through substrate
% See Griffiths "Intro to Electrodynamics 3rd Ed. Eq. 9.86 &
9.87
T_glass=abs(4*1*n(1,:)./(1+n(1,:)).^2);
R_glass=abs((1-n(1,:))./(1+n(1,:))).^2;

t = thicknesses;
t(1)=0;
Jsc=0*VaryThickness;

%% AT EACH LAYER THICKNESS THAT IS VARIED %%%%%%%%%%%%%%%%
forThickInd= 1:length(VaryThickness)
t(LayerVaried)=VaryThickness(ThickInd)
% Calculate transfer matrices, and field at each wavelength
and position

t_cumsum=cumsum(t);
x_pos=(stepsize/2):stepsize:sum(t); %positions to evaluate
field
%   x_mat specifies what layer number the corresponding point
in x_pos is in:
x_mat=
sum(repmat(x_pos,length(t),1)>repmat(t_cumsum',1,length(x_pos)
),1)+1;
    R=lambda*0;
    E=zeros(length(x_pos),length(lambda));
for l = 1:length(lambda)
% Calculate transfer matrices for incoherent reflection and
transmission at the first interface
        S=I_mat(n(1,l),n(2,l));
formatindex=2:(length(t)-1)
```

```
S=S*L_mat(n(matindex,l),t(matindex),lambda(l))*I_mat(n(matinde
x,l),n(matindex+1,l));
end
R(l)=abs(S(2,1)/S(1,1))^2; %JAP Vol 86 p.487 Eq 9 Power
Reflection from layers other than substrate
T(l)=abs(2/(1+n(1,l)))/sqrt(1-R_glass(l)*R(l)); %Transmission
of field through glass substrate Griffiths 9.85 + multiple
reflection geometric series

% Calculate all other transfer matrices
for material = 2:length(t)
xi=2*pi*n(material,l)/lambda(l);
dj=t(material);
x_indices=find(x_mat == material); %indices of points which
are in the material layer considered
            x=x_pos(x_indices)-t_cumsum(material-1); %distance
from interface with previous layer
% Calculate S matrices (JAP Vol 86 p.487 Eq 12 and 13)
S_prime=I_mat(n(1,l),n(2,l));
formatindex=3:material
                S_prime=S_prime*L_mat(n(matindex-
1,l),t(matindex-1),lambda(l))*I_mat(n(matindex-
1,l),n(matindex,l));
end
S_doubleprime=eye(2);
formatindex=material:(length(t)-1)

S_doubleprime=S_doubleprime*I_mat(n(matindex,l),n(matindex+1,l
))*L_mat(n(matindex+1,l),t(matindex+1),lambda(l));
end
% Normalized Field profile (JAP Vol 86 p.487 Eq 22)
            E(x_indices,l)=T(l)*(S_doubleprime(1,1)*exp(-
1i*xi*(dj-x))+S_doubleprime(2,1)*exp(1i*xi*(dj-x)))
./(S_prime(1,1)*S_doubleprime(1,1)*exp(-
1i*xi*dj)+S_prime(1,2)*S_doubleprime(2,1)*exp(1i*xi*dj));
end
end

% Absorption coefficient in cm^-1 (JAP Vol 86 p.487 Eq 23)
    a=zeros(length(t),length(lambda));
formatindex=2:length(t)
a(matindex,:)=4*pi*imag(n(matindex,:))./(lambda*1e-7);
end

% Calculate 100% IQE current achieved with device

% Energy dissipation mW/cm3-nm at each position and wavelength
(JAP Vol 86 p.487 Eq 22)
ActivePos=find(x_mat == activeLayer);
```

```
Q=repmat(a(activeLayer,:).*real(n(activeLayer,:)).*AM15,length
(ActivePos),1).*(abs(E(ActivePos,:)).^2);

% Exciton generation rate per second-cm3-nm at each position
and wavelength
Gxl=(Q*1e-3).*repmat(lambda*1e-9,length(ActivePos),1)/(h*c);
if length(lambda)==1
lambdastep= 1;
else
lambdastep=(max(lambda)-min(lambda))/(length(lambda)-1);
end
Gx=sum(Gxl,2)*lambdastep; % Exciton generation rate as a
function of position/(sec-cm^3)

% outputs predicted Jsc under AM1.5 illumination assuming 100%
internal
% quantum efficiency at all wavelengths
Jsc(ThickInd)=sum(Gx);%;*stepsize*1e-7*q*1e3; %in mA/cm^2
%Jsc=Gx;

end
plot(VaryThickness, Jsc)
title('Current Density obtained from 100% IQE')
xlabel('Layer thickness (nm)')
ylabel('Current Density (mA/cm^2)')
assignin('base','Thickness',VaryThickness);
assignin('base','Jsc',Jsc);

%------------------- Helper Functions -----------------------
------------
% Function I_mat
% This function calculates the transfer matrix, I, for
reflection and
% transmission at an interface between materials with complex
dielectric
% constant n1 and n2.
function I = I_mat(n1,n2)
r=(n1-n2)/(n1+n2);
t=2*n1/(n1+n2);
I=[1 r; r 1]/t;

% Function L_mat
% This function calculates the propagation matrix, L, through
a material of
% complex dielectric constant n and thickness d for the
wavelength lambda.
function L = L_mat(n,d,lambda)
xi=2*pi*n/lambda;
L=[exp(-1i*xi*d) 0; 0 exp(1i*xi*d)];
```

```
% Function LoadRefrIndex
% This function returns the complex index of refraction
spectra, ntotal, for the
% material called 'name' for each wavelength value in the
wavelength vector
% 'wavelengths'.  The material must be present in the index of
refraction
% library 'Index_of_Refraction_library.xls'.  The program uses
linear
% interpolation/extrapolation to determine the index of
refraction for
% wavelengths not listed in the library.
functionntotal = LoadRefrIndex(name,wavelengths)

%Data in IndRefr, Column names in IndRefr_names
[IndRefr,IndRefr_names]=xlsread('Indeex_of_Refraction_library.
xls');

% Load index of refraction data in spread sheet, will crash if
misspelled
file_wavelengths=IndRefr(:,strmatch('Wavelength',IndRefr_names
));
n=IndRefr(:,strmatch(strcat(name,'_n'),IndRefr_names));
k=IndRefr(:,strmatch(strcat(name,'_k'),IndRefr_names));

% Interpolate/Extrapolate data linearly to desired wavelengths
n_interp=interp1(file_wavelengths, n, wavelengths, 'linear',
'extrap');
k_interp=interp1(file_wavelengths, k, wavelengths, 'linear',
'extrap');

%Return interpolated complex index of refraction data
ntotal = n_interp+1i*k_interp;
```

ELECTRICAL MODEL CODE:

```
mun00=2.5*10^-7;
mup00=3*10^-8;
Eg=1.3;
k=1.38*10^-23;
T=300;
diel_r=10^-11;
diel_0=3;
Vbegin=0;
dV=0.1;
En00=2*10-3;
Ep00=En00;
althick=100;
a1thick=100;
Nc=2.5*10^25;
Nv=Nc;
l=1;
dl=1;
q=1.6*10^-19;
d1=dl;
O=0;
kT=k*T;
ts_factor=1;
G2=2.7*10^27;
kf=1.5*10^6;
%588
Ep0=Ep00*ones(althick+2,1);En0=En00*ones(althick+2,1);
mun0=mun00*ones(althick+2,1); mup0=mup00*ones(althick+2,1);

FF=0; pmax=0; Vpmax=0; Jpmax=0; Jsc=0; Joc=100;
Voc=0; Vocbot=0; Voctop=0;Jocbot=1000; Joctop=1000;
p=zeros(althick+2,1); n=zeros(althick+2,1);
F=zeros (althick+2,1); Fint=zeros (althick+2,1);
pnew=zeros(althick+2,1) ;nnew=zeros(althick+2,1);
Xnew=zeros(althick+2,1) ; X=zeros (althick+2, 1) ;
 R=zeros (althick+2,1) ; P=zeros (althick+2, 1) ;
U=zeros (althick+2, 1) ;jp=zeros (althick+2, 1) ; jn=zeros
(althick+2, 1) ;
jt=zeros(althick+2,1) ; jpdiff=zeros (althick+2 , 1);
jpdrift=zeros(althick+2,1) ;
jndrift=zeros(a1thick+2, 1); jndiff=zeros(althick+2, 1);
mun=zeros(althick+2,1) ; mup=zeros(althick+2, 1);
Dp=zeros (althick+2, 1) ;Dn=zeros (althick+2, 1) ;

nisq=Nc*Nv*exp(-Eg/(k*T)) ;
p(3:althick)=4e17;
n(3:althick)=4e17;
```

```
V=Vbegin:dV:0.7;

foryy=1:length(V)

VV=V(yy);
p(2)=Nv; p(althick+l)=Nv*exp(-Eg/(k*T));
n(2)=Nc*exp(-Eg/(k*T)); n(althick+l)= Nc;
%589
p(1)=n(2);n(1)=p(2);
p(a1thick+2)=n(althick+1);
n(a1thick+2)=p(althick+1);
flag=0;
% Electrical Field Calculation
for mm= l:althick+l
Fint(mm)=0;
for pp=1:a1thick+2
if pp<=mm
Fint(mm)=Fint(mm)+dl*q*(p(pp)-n(pp))/2/diel_0/diel_r;
else
Fint(mm)=Fint(mm)-dl*q*(p(pp)-n(pp))/2/diel_0/ diel_r;
end
end
end
for mm=2:althick+l
F(mm)=(Fint(mm-l)+Fint(mm))/2;
end
VF=sum(F.*dl) ;
%VF=Vbi+VF;
n(l)=n(l)+(VF-VV)*diel_0*diel_r/(q*dl*althick*dl) ;
p(althick+2) =p(althick+2)+(VF-
VV)*diel_0*diel_r/(q*dl*althick*d1);
if n(1)<p(l)
p(1)=p(1)-n(1) ;n(1)=0;
else
n(1)=n(1)-p(1) ;p(1)=O;
%590
end

if n(althick+2)<p(althick+2)
p(althick+2)=p(althick+2)-n(althick+2);n(althick+2)=0;
else
n(althick+2)=n(althick+2)-p(althick+2);p(althick+2)=0 ;
end

for mm=2:althick+l
F(mm)=F(mm)-(VF-VV)/althick/dl;
mun(mm)=mun0(mm)*exp(En0(mm)*sqrt(abs(F(mm))));
Dn(mm)=mun(mm)*kT;

mup(mm)=mup0(mm)*exp(Ep0(mm)*sqrt(abs(F(mm))));
Dp(mm)=mup(mm)*kT;
```

```
end

F;

x=[abs(mun.*F); abs(mup.*F);abs(Dn/dl);abs(Dp/dl)];
mufmax=max(max(x));
dt=dl/mufmax/ts_factor;
Nmax=100;
foriter=l:Nmax

iter;flag;yy;
if flag==O

flag=l;
dpp=O;dnn=O;

for gg=3:althick
    pnew(gg)=p(gg)+dt*((Dp(gg+l)*p(gg+l)+Dp(gg-l)*p(gg-l)-
2*Dp(gg)*p(gg))); %check for error
if (F(gg+l)<O)
pnew(gg)=pnew(gg)+dt*p(gg+l)*mup(gg+l)*abs(F(gg+l))/dl;
%591
end
if (F(gg-1)>0)
pnew(gg)=pnew(gg)+dt*p(gg-1)*mup(gg-1)*abs(F(gg-l))/dl;
end
nnew(gg)=n(gg)+dt*((Dn(gg+1)*n(gg+1)+Dn(gg-1)*n(gg-1)-
2*Dn(gg)*n(gg))); %check for error

if (F(gg+1)>0)
nnew(gg)=nnew(gg)+dt*n(gg+l)*mun(gg+l)*abs(F(gg+1))/dl;
end
if (F(gg-1)<0)
nnew(gg)=nnew(gg)+dt*n(gg-l)*mun(gg-1)*abs(F(gg-1))/dl;
end
end
gg=2;
pnew(gg)=p(gg)+dt*((Dp(gg+l)*p(gg+l)-Dp(gg)*p(gg))/(dl*dl));
if (F(gg+1)<0)
pnew (gg)=pnew(gg)+dt*p(gg+1)*mup(gg+1)*abs(F(gg+l))/dl;
end
if (F(gg) >0)
pnew(gg)=pnew(gg)-dt*p(gg)*mup(gg)*abs(F(gg))/dl;
end
nnew(gg)=n(gg)+dt*((Dn(gg+l)*n(gg+l)-Dn(gg)*n(gg))/(dl*dl));
if (F(gg+l)>O)
nnew(gg)=nnew(gg)+dt*n(gg+l)*mun(gg+l)*abs(F(gg+l))/dl;
end
if (F(gg)<O)
nnew(gg)=nnew(gg)-dt*n(gg)*mun(gg)*abs(F(gg))/dl;
```

```
end
%592
gg=althick+1 ;
pnew(gg)=p(gg)+dt*((Dp(gg-1)*p(gg-1)-Dp(gg)*p(gg))/(dl*dl)) ;
if (F(gg-l)>0)
pnew(gg)=pnew(gg)+dt*p(gg-1)*mup(gg-1)*abs(F(gg-1))/dl ;
end
if (F (gg) <0)
pnew(gg)=pnew(gg)-dt*p(gg)*mup(gg)*abs(F(gg))/dl;
end
nnew(gg)=n(gg)+dt*((Dn(gg-1)*n(gg-1)-Dn(gg)*n(gg))/(dl*dl)) ;
if (F(gg-l)<O)
nnew(gg)=nnew(gg)+dt*n(gg-1)*mun(gg-1)*abs(F(gg-1))/dl ;
end
if (F(gg)>0)
nnew(gg)=nnew(gg)-dt*n(gg)*mun(gg)*abs(F(gg))/dl;
end
for gg=2:althick+1
if (n(gg)*p(gg))>nisq
R(gg)=q*(mun(gg)+mup (gg))*(n(gg)*p(gg)-nisq)/diel_0/diel_r;
else
R(gg)=0;
end
Xnew(gg)=X(gg)+dt*(G2(gg-1)/(dl*q*1000)-kf*X(gg)-
kd(mun(gg)+mup (gg))); %error

pnew(gg)=pnew(gg)-R(gg)*dt+kd (mun(gg)+mup (gg),a, diel_r ,F
(gg)) *X (gg); %error
nnew(gg)=nnew(gg)-R(gg) *dt+kd (mun (gg) +mup (gg) ,a,diel_r
,F(gg) )*X(gg); %eror
P(gg)=kd(mun(gg)+mup(gg),a,diel_r,F(gg))/(kd(mun(gg)+mup(gg),a
,diel_r)); %error

U(gg)=P(gg)*G2(gg-1)/(dl*q*1000)-(l-P(gg))*R(gg);
end
%593
p(1)=p(1)+n(2)-nnew(2);
n(1)=n(1)+p(2)-pnew(2);
p(althick+2)=p(althick+2)+n(althick+1)-nnew(althick+1);
n(althick+2)=n(althick+2)+p(althick+l)-pnew(althick+l);
xcheck(iter)=p(8);xcheckl(iter)=n(8) ;
if flag==1
for gg=2:althick+1
if abs(Xnew(gg)-X(gg))>abs(converge*dt*XnQw(gg))
flag=0;
end
end
end
if flag==l
for gg=3:althick
if abs(pnew(gg)-p(gg))>abs(converge*dt*pnew(gg))
```

```
flag=0;
end
if abs(nnew(gg)-n(gg))>abs(converge*dt*nnew(gg))
flag=0;
end
end
end
if flag==1
jp(1)=(p(2)-pnew(2))*dl*q*1000/dt;
jn(1)=-(n(2)-nnew(2))*dl*q*1000/dt;
jt(1)=jp(1)+jn(1);
jp(althick+1)=-(p(althick+1)-pnew(althick+1))*dl*q*1000/dt;
%594
jn(althick+1)=(n(althick+1)-nnew(althick+1))*d1*q*1000/dt;
jt(althick+1)=jp(althick+1)+jn(althick+1) ;
if abs(jt(1)-
jt(althick+1))>abs(converge*(abs(jt(althick+1))+abs(jt)));%err
or
flag=0;
end
for gg=2:althick
dpp=dt*(Dp(gg)*p(gg)-Dp(gg+1)*p(gg+1))/(dl*dl);
jpdiff(gg)=dpp*dl*q*1000/dt;
dpp=0;
if (F(gg) >0)
dpp=dt*p(gg)*mup(gg)*abs(F(gg))/dl ;
end
if (F(gg+1)<0)
dpp=dpp-dt*p(gg+1)*mu(pgg+1)*abs(F(gg+1))/d1;
end
jpdrift(gg)=dpp*dl*q*1000/dt;
dnn=dt*(Dn(gg)*n(gg)-Dn(gg+1)*n(gg+1))/(dl*dl);
jndiff(gg)=-dnn*dl*q*1000/dt;
dnn=O;
if (F(gg)<0)
dnn=dt*n(gg)*mun(gg)*abs(F(gg))/dl;
end
if (F(gg+1)>O)
dnn=dnn-dt*n(gg+1)*mun(gg+1)*abs(F(gg+1))/dl;
end
jndrift(gg)=-dnn*dl*q*1000/dt;
%595
jp(gg)=jpdiff(gg)+jpdrift(gg);
jn(gg)=jndiff(gg)+jndrift(gg);
jt(gg)=jp(gg)+jn(gg) ;

end

end

for gg=3:althick
```

```
p(gg)=pnew(gg);n(gg)=nnew(gg);
X(gg)=Xnew(gg) ;

end

X(2)=Xnew(2);
X(althick+l)=Xnew(althick+l) ;

%Electrical Field Calculation
for mm=l:althick+l
Fint (mm)=0 ;
for pp=1:althick+2
if pp<=mm
Fint (mm)=Fint(mm)+dl*q*(p(pp)-n(pp))/2/diel_0/diel_r;

else

Fint (mm)=Fint(mm)-dl*q*(p(pp)-n(pp))/2/diel_0/diel_r;

end

end

end
for mm=2:althick+l
F(mm)=(Fint(mm-l)+Fint(mm))/2;
end
VF=sum(F.*dl);

%596
VF=Vbi+VF;
n(1)=n(1)+(VF-VV)*diel_0*diel_r/(q*dl*althick*dl);

p(althick+2) =p(althick+2)+(VF-
VV)*diel_0*diel_r/(q*dl*althick*dl);
if n(l)<p(l)
P(1)=p(1)-n(1);n(1)=0;
else
n(l)=n(l)-p(1);p(l)=0;

end

if n(althick+2)<p(althick+2)
p(althick+2)=p(althick+2)-n(althick+2);n(althick+2)=0;
else
n(althick+2)=n(althick+2)-p(althick+2);p(althick+2)=0;

end

for mm=2:althick+l
```

```
F(mm)=F(mm)-(VF-VV)/althick/dl;

mun(mm)=mun0(mn)*exp(En0(mm)*sqrt(abs(F(mm))));
Dn(mm)=mun(mm)*kT;
mup(mm)=mup0(mm)*exp(Ep0(mm)*sqrt(abs(F(mm))))  ;
Dp(mm)=mup(mm)*kT;

end

x=[abs(mun.*F); abs(mup.*F)  ;abs(Dn/dl)  ;abs(Dp/dl)];
mufmax=max(max(x));
dt=dl/mufmax/ts_factor;

elsebreak

end

end

if flag==0
jp (1)=(p(2)-pnew(2))*dl*q*1000/dt;
jn(1) =-(n(2)-nnew(2))*dl*q*1000/dt;
%597
jt(1)=jp(1)+jn(1) ;

jp(althick+1)=-(p(althick+l)-pnew(althick+1) )*dl*q*1000/dt;
jn(althick+l)=(n(althick+l)-nnew(althick+1))*dl*q*1000/dt;
jt (althick+l)=jp(althick+l)+jn(althick+l) ;
if abs(jt(l)-
jt(althick+l))>abs(converge*(abs(jt(althick+l))+abs(jt(1))));%
error
flag=0;
end

for gg=2: althick

dpp=dt*(Dp(gg)*p(gg)-Dp(gg+ 1)*p(gg+1))/ (dl*dl);
jpdiff (gg)=dpp*dl*q*1000/dt;

dpp=0;
if (F (gg)>0)
dpp=dt*p (gg)*mup(gg)*abs (F(gg))/dl ;

end

if (F(gg+1)<0)
dpp=dpp-dt*p(gg+1)*mup(gg+l)*abs(F(gg+1))/dl;
end

jpdrift(gg)=dpp*dl*q*1000/dt;
```

```
dnn=dt*(Dn(gg)*n(gg)-Dn(gg+l)*n(gg+l))/(dI*dI);
jndiff(gg)=-dnn*dl*q*1000/dt;

dnn=0;

if (F(gg)<0)
dnn=dt*n(gg)*mun(gg)*abs(F(gg))/dl ;

end
if (F(gg+l)>0)

%598
dnn=dmm-dt*n(gg+1)*mun(gg+1)*abs(F(gg+ 1))/dl;
end
jndrift(gg)=-dnn*dl*q*1000/dt;
jp(gg)=jpdiff(gg)+jpdrift(gg);
jn(gg)=jndiff(gg)+jndrift(gg);
jt(gg)=jp(gg)+jn(gg) ;
end
end
power(yy)=0;
power(yy)=-VV*jt(1); Ji(yy)=jt(1); Jf(yy)=jt(althick+1);
if((VV>0) && (power(yy)>pmax))
pmax=power(yy) ; Vpmax=VV; Jpmax=jt(l) ;
end
if (abs(VV)<1.0e-3)
Jsc=jt(1) ;
end
if(VV>=0 &&jt(1)<0 && abs(jt(1))<abs(Jocbot))
Jocbot=jt(1) ;Vocbot=VV;
end
if(VV>=0 &&jt(l)>O && abs(jt(1))<abs(Joctop))
Joctop=jt(1) ;Voctop=VV;
end
end
Voc=(Joctop*Vocbot-Jocbot*Voctop)/(Joctop-Jocbot);
Jsc=abs(Jsc) ;
FF=pmax/(Jsc*Voc) ;
%599
figure(2)
plot(V,Ji(1:9));
```